



# UNIVERSITY OF TWENTE.

Faculty of Electrical Engineering,  
Mathematics & Computer Science

## Interference Nulling via a Resistor-Weighted Op-Amp Vector Modulator

Frederik van den Ende  
Master of Science Thesis  
March 2011

---

### Supervisors

ir. M.C.M. Soer  
dr. ing. E.A.M. Klumperink  
prof. dr. ir. F.E. van Vliet

Report number: 067.3400  
Chair of Integrated Circuit Design  
Faculty of Electrical Engineering,  
Mathematics and Computer Science  
University of Twente  
P.O. Box 217  
7500 AE Enschede  
The Netherlands

---





## Abstract

In order to perform interference nulling (through beamforming), for an interferer with variable angular position, the radiation pattern of an array antenna has to be adjusted electronically.

This thesis deals with a beamforming algorithm that rotates the beams of a Butler Matrix beamforming network (BFN), such that one of the beams is able to 'capture' an interferer. This beam is strongly attenuated, such that the interferer is nulled out. In this way the signal-to-interference ratio (SIR) is improved. Subsequently, a vector modulator performs phase shifting in order to optimize the signal-to-noise ratio (SNR).

Based on an existing platform, a circuit level implementation, using Op-Amps and resistors, is proposed to verify the nulling performance of the beamforming algorithm.

Circuit simulations demonstrate, for low resolutions, a minimum rejection of 17.56 dB, such that the SIR is improved by this number.



# Contents

<b>1</b>	<b>Introduction</b>	<b>1</b>
1.1	Beamforming	2
1.1.1	Antenna Array Basics	2
1.1.2	Complex Weights	3
1.2	Project Description	3
1.3	Previous Work	4
1.4	Idea	5
1.5	Research Questions	5
1.6	Acknowledgements	6
1.7	Outline	6
<b>2</b>	<b>Interference Nulling</b>	<b>7</b>
2.1	Multiple Beams	7
2.2	Butler Matrix	7
2.3	Motivation for the Butler Matrix	9
2.4	Analysis of the Butler Matrix	10
2.4.1	Beam Position	10
2.4.2	Phase Progression	11
2.4.3	Matrix Synthesis & Orthogonality	11
2.5	Beam Summation	13
2.6	Beam Cancellation	14
2.7	Broadside Butler	15
2.8	Beamforming Function	16

<b>3</b>	<b>Beamforming Algorithm</b>	<b>19</b>
3.1	Howells-Applebaum Algorithm . . . . .	19
3.2	Synthesis of the Complex Weights . . . . .	21
3.3	2-Step Beamforming . . . . .	23
3.3.1	Beam Weighting . . . . .	23
3.3.2	SNR Optimization . . . . .	25
<b>4</b>	<b>Beamforming Platform</b>	<b>27</b>
4.1	System Functions . . . . .	27
4.2	Motivation . . . . .	28
4.2.1	Mixer Array . . . . .	29
4.2.2	TIA Stages . . . . .	29
4.2.3	Linearity . . . . .	30
<b>5</b>	<b>System Model Evaluation</b>	<b>31</b>
5.1	Circuit Constraints . . . . .	31
5.1.1	Butler Beamforming Network . . . . .	31
5.1.2	Weight Quantization . . . . .	32
5.2	Model Simulations . . . . .	32
5.2.1	Quantized Butler Phases . . . . .	32
5.2.2	Quantized Magnitude Weights . . . . .	34
5.2.3	Quantized Phase Weights . . . . .	34
<b>6</b>	<b>Circuit Level Design</b>	<b>37</b>
6.1	Beamforming Front-End . . . . .	37
6.2	Mixer Block . . . . .	38
6.3	Butler BFN . . . . .	39
6.4	TIA Stage . . . . .	40
6.4.1	Proposed Circuit Implementation . . . . .	40
6.4.2	Transimpedance . . . . .	41
6.4.3	MOST Switches . . . . .	41

## CONTENTS

6.4.4	Charge Pump . . . . .	42
6.4.5	Bandwidth . . . . .	43
6.5	Vector Modulator . . . . .	43
6.5.1	Vector Modulation . . . . .	44
6.5.2	Synthesis of the Weights . . . . .	45
6.5.3	Implementation of the Weights . . . . .	46
6.5.4	Proposed Vector Modulator Implementation . . . . .	47
<b>7</b>	<b>Simulation Results</b>	<b>49</b>
7.1	Simulation Setup . . . . .	49
7.2	Gain Compression . . . . .	50
7.3	Third-Order Intermodulation Distortion . . . . .	51
7.4	Vector Modulator . . . . .	52
7.5	Nulling Performance . . . . .	53
7.6	A Word about Noise . . . . .	54
7.7	Power Consumption . . . . .	54
<b>8</b>	<b>Conclusions</b>	<b>55</b>
<b>9</b>	<b>Recommendations</b>	<b>57</b>
	<b>Bibliography</b>	<b>60</b>



# Chapter 1

## Introduction

Nowadays the radio-frequency (RF) spectrum becomes increasingly filled with transmitters operating in the same frequency-band. Modern radio receivers need to support a variety of (mobile) communication standards, each using a different frequency-band. Due to this 'crowded' spectrum, receivers need to accommodate quite a few highly selective analog filters in order to select the right frequency-band.

High-order analog filters typically operate in a single fixed frequency-band. This is undesired for upcoming applications, such as software-defined radio (SDR) and cognitive radio (CR), which require a high degree of flexibility.

Cognitive radio operates in unused spots in the frequency spectrum. Fixed transmitters (e.g. TV channels) are closely spaced to these empty spots and are considerably stronger. Strong interferers, nearby the wanted signal (band), are hard to reject by means of frequency-domain filtering. Still, these blocking signals or *blockers* can desensitize the receiver.

Consider Figure 1.1 where a piece of unused spectrum (between two strong interferers) is available for cognitive radio applications. A band-pass filter might be used to select this 'piece of spectrum'.

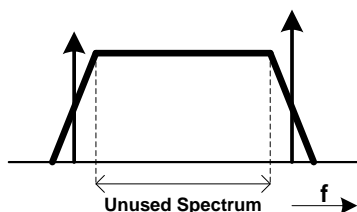


Figure 1.1: Unused spectrum in between two strong interferers.

Although the interferers are located outside the passband of this filter, they cannot be suppressed adequately, due to the finite steepness of the band filter. Therefore another approach should be exploited, in order to reject these kind of strong interferers.

## 1.1 Beamforming

Antennas can be configured as an array of antenna-elements. When the signals from these elements are amplified and/or phase-shifted and subsequently summed, the radiation pattern is modified. In this way the radiation pattern of the array can be adjusted electronically. This is called *beamforming*. Beamforming is also referred to as spatial filtering. If, as in the case of Figure 1.1, a wanted signal and an interferer are spatially separable, it might be possible to obtain sufficient rejection. Beamforming can also be used in order to increase the signal-to-noise ratio (SNR).

### 1.1.1 Antenna Array Basics

Consider a linear array of  $K$  omnidirectional equally spaced radiators. It is assumed that the radiators have an isotropic radiation pattern and mutual coupling between the elements is neglected for simplicity. Consequently, the radiation pattern of the array is described by the array factor (F) [Visser, 2005, p. 127], that is:

$$F(\theta) = \sum_{i=1}^K e^{jk_0(i-1)d\sin(\theta)} \quad (1.1)$$

where

$$k_0 = \frac{2\pi}{\lambda_0}$$

- $\lambda_0$  is the wavelength in free space.
- $k_0$  is the angular wave number in free space, i.e. the magnitude of the wave vector.
- $d$  is the inter-element distance.
- $\theta$  is the angle relative to the array normal (broadside or z-direction).

So, when the contributions from the elements are summed, the radiation pattern of the array is obtained. In Figure 1.2b the radiation pattern of a 4-element linear array with  $\frac{1}{2}\lambda_0$  inter-element spacing ( $d$ ) is plotted.

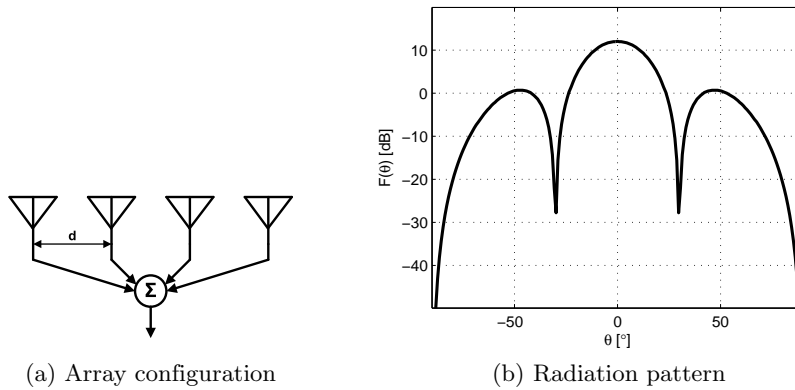


Figure 1.2: Configuration and radiation pattern of a 4-element linear array.

The radiation pattern is plotted for  $\theta = [-90^\circ \dots 90^\circ]$ , i.e. visible space, because the array factor for the interval  $\theta = [90^\circ \dots 270^\circ]$  is mirrored with respect to the interval  $\theta = [-90^\circ \dots 90^\circ]$ .

### 1.1.2 Complex Weights

In the expression for the array factor (1.1), it is assumed that the amplitudes received by the elements of the array are equal. That is, the array exhibits a uniform aperture distribution. It is also assumed that the summation network introduces no additional phase differences or time delays.

Most array systems incorporate 'weights' in order to perform beamforming. These weights can provide amplification and/or phase shifting. Hence the name *complex weights*. Amplitude weighting is often referred to as *amplitude tapering* [Visser, 2005, §4.6]. An amplitude taper lowers the sidelobe level at the cost of broadening the main beam. *Phase tapers* are used to phase shift the antenna signals such that they coherently add up. In this way, the SNR can be improved for a certain direction of arrival, as in the case of a *Phased Array*.

## 1.2 Project Description

This thesis examines the feasibility of implementing a beamforming system to perform *interference nulling*. This work is performed in the framework of beamforming for consumer electronics, i.e. personal communications for frequencies of 1 - 5 GHz.

At system level it is investigated if beamforming is suitable to perform interference nulling according to some specifications. Subsequently, a possible implementation of the beamforming system is examined at circuit level.

### 1.3 Previous Work

In previous work [Soer et al., 2011], a beamforming system based on a *Vector Modulator* was proposed. A vector modulator performs phase shifting and/or amplification, by modulating the magnitudes of two quadrature phases (orthogonal vectors) and summing the results.

Consider Figure 1.3. Summing two orthogonal vectors, i.e. I & Q, yields the resulting vector, which experiences a phase shift with respect to I & Q. In this way the complex weights can be adjusted in order to steer a beam to a desired direction.

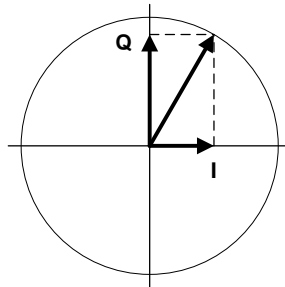


Figure 1.3: Phasor Diagram.

[Wang and Hajimiri, 2007] presented a digital linear *Phase Rotator*, in which the I & Q components of the local oscillator (LO) signal each serve as input to a variable gain amplifier (VGA). These VGAs are transconductor stages, sensing the LO signal and producing an output current. Their gains are 5 bit digitally controlled and can be set independently from each other. Adding the outputs of the VGAs in the current domain results in an interpolated signal with the desired phase and amplitude.

[Rackowski et al., 2010] reported a wideband beamformer, in which the output currents of a quadrature mixer serve as input to a phase shifter. These phase shifters are implemented using 4 digitally controlled variable-gain current amplifiers, as currents are easily summed to produce the phase-shifted output signal. The phase shifts are derived from a lookup table, which contains the gains of a single VGA.

The complex weights of the beamforming system proposed by [Soer et al., 2011] were implemented using capacitor ratios. In this work, an alternative idea is investigated to realize a beamforming system in order to perform interference nulling.

## 1.4 Idea

In this work the implementation of complex weights *based on the combination of Op-Amps and resistors* is examined. This could save power consumption and die area compared to using capacitors as in [Soer et al., 2011]. Consider Figure 1.4.

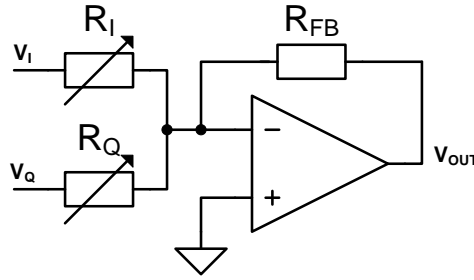


Figure 1.4: Possible implementation of a *Vector Modulator*.

The voltages  $V_I$  &  $V_Q$ , which are  $90^\circ$  out of phase (i.e. I/Q signals), are converted to current through the variable resistors and added at the summation node at the inverting input of the Op-Amp. Subsequently the summed current flows through the feedback resistor ( $R_{FB}$ ) and hence converted back to voltage. So the resulting voltage ( $V_{OUT}$ ) experiences a phase shift with respect to the input voltages. In this way a vector modulator can be constructed.

This work examines if the implementation of complex weights, using resistors and Op-Amps, is suitable for a beamforming algorithm in order to perform interference nulling. This leads to the following research questions.

## 1.5 Research Questions

1. Given a linear phased array configuration, can the radiation pattern be adjusted in a structured way to perform interference nulling (with sufficient accuracy) through beamforming?
2. Based on the proposed beamforming system, is an Op-Amp implementation with resistive feedback feasible for synthesizing the complex weights necessary to generate the desired radiation pattern?

## 1.6 Acknowledgements

First of all, I would like to thank Michiel Soer for providing me with this assignment. It was challenging & versatile, ranging from array theory to pattern synthesis and from front-end design considerations to Op-Amp circuits. Also his help considering circuit simulations is acknowledged.

Secondly, I would like to thank Eric Klumperink for his feedback on behalf of writing this thesis and the discussions considering the circuit implementations. Also I want to thank Remko Struiksma for his critical review of this report. I would like to thank professor Bram Nauta, for facilitating this graduation project carried out within the ICD group of the University of Twente and professor Frank van Vliet for leading the graduation committee. Furthermore I want to thank the (former) ICD students, especially Michiel Duiven for the nice cooperation during our studies.

My thank goes out to my parents, who gave me the opportunity to study and supported me during my whole study period. Finally I would like to thank Inge van Leeuwenkamp for her love and patience during the last months.

## 1.7 Outline

This thesis is organized as follows:

- Chapter 2 introduces a beamforming network (BFN), which is used to perform interference nulling in a structured way.
- Chapter 3 describes a beamforming algorithm, which performs interference nulling and SNR improvement.
- Chapter 4 examines an existing platform for the beamforming system.
- Chapter 5 evaluates the performance of the system model, due to constraints imposed by a circuit implementation.
- Chapter 6 proposes circuit implementations, suitable for synthesizing the complex weights of the beamforming system.
- Chapter 7 provides simulation results, obtained with SpectreRF.
- Chapter 8 presents the conclusions.
- Chapter 9 offers some recommendations.

## Chapter 2

# Interference Nulling

### 2.1 Multiple Beams

As elucidated in Chapter 1, the main function of the beamforming system is to perform interference nulling. It is hereby assumed, that the angular position of the interferer, which is random, is known a priori. However, in the absence of interference the array should be sensitive in all directions. As depicted in Figure 1.2b, the array is most sensitive in broadside direction (i.e.  $0^\circ$ ), whereas in endfire direction (i.e.  $\pm 90^\circ$ ) the array is not sensitive at all. The four-element array has natural pattern nulls at  $\pm 30^\circ$ . If an incoming signal enters the array at an angle of  $\pm 30^\circ$  or  $\pm 90^\circ$ , the array will not notice its presence.

In order to satisfy these *sensitivity conditions*, multiple beams are needed. Multiple beams can be created by means of a beamforming network (BFN) or via quasi-optical lenses [Hansen, 2009, §10.2]. The latter is not further described here. The next section introduces an often used BFN.

### 2.2 Butler Matrix

A *Butler Matrix*<sup>1</sup>, named after his inventor [Butler and Lowe, 1961], is a beamforming network, which can mathematically be represented by a square matrix:

$$\begin{bmatrix} 0^\circ & -45^\circ & -90^\circ & -135^\circ \\ -90^\circ & 45^\circ & 180^\circ & -45^\circ \\ -45^\circ & 180^\circ & 45^\circ & -90^\circ \\ -135^\circ & -90^\circ & -45^\circ & 0^\circ \end{bmatrix} \quad (2.1)$$

---

<sup>1</sup>Within this work, this beamforming network is referred to as *Butler BFN*, while the mathematical representation - as in (2.1) - is referred to as *Butler matrix*, even though a Butler matrix is in fact a type of beamforming network!

In Figure 2.1 an often encountered representation of a Butler BFN is given [Litva and Lo, 1996, §2.2] [Rajagopalan, 2006].

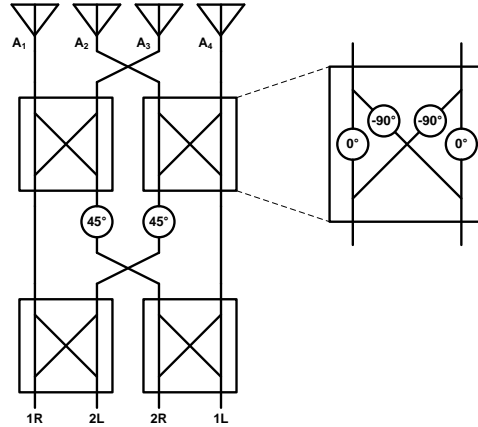
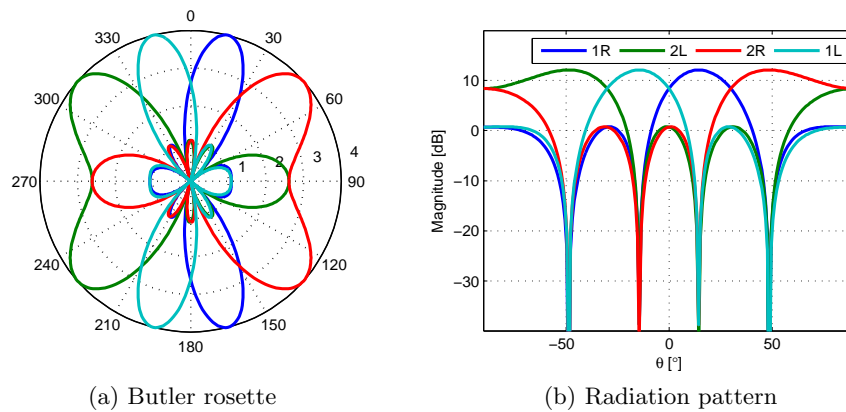


Figure 2.1: Antenna array feeding a Butler BFN.

The BFN in Figure 2.1 consists of 4 hybrid junctions and 2 fixed phase shifters. A 4-element array antenna feeds the upper hybrid junctions, which perform a  $-90^\circ$  phase shift when a signal propagates to the other branch in the hybrid. The outputs of the lower hybrids are referred to as *beam ports*. A Butler BFN connects  $N = 2^n$  (where  $n = 1, 2, 3, \dots$ ) array elements to an equal number of beam ports. The signals present at these beam ports represent a beam. The Butler BFN in Figure 2.1 results 4 beams, which are shown in Figure 2.2.



(a) Butler rosette

(b) Radiation pattern

Figure 2.2: Butler beams.

As becomes clear from Figure 2.2, 1R represents the first beam positioned right from broadside direction. 2L represents the second beam positioned left from broadside direction, and so on. . .

A Butler BFN is often recognized as the calculation flowchart (a.k.a. *FFT butterfly*) of the fast Fourier transform (FFT) [Hansen, 2009, §10.2.1.2] [Mailloux, 2005, §1.3.2]. From this point of view, it could be said that a Butler BFN performs a *spatial* fast Fourier transform. That is, the Butler BFN performs an FFT on a discrete number of antenna elements, giving a discrete number of 'direction of arrival' bins.

## 2.3 Motivation for the Butler Matrix

Next to the *Butler Matrix* in the general sense, there exists other types of beamforming networks, such as the *Blass Matrix* and the *Nolen Matrix* [Hansen, 2009, §10.2.1.3]. A 'classical' Blass matrix BFN uses a set of array-element transmission lines, which intersect a set of beam port lines via power dividers to generate multiple beams. The Blass matrix BFN can have a number of beam ports *unequal* to the number of antenna elements.

The Nolen matrix BFN is in fact a generalization of both the Butler and the Blass matrices, such that the Nolen matrix can be reduced to the Butler matrix when  $N = 2^n$ . Just like the Butler BFN can be considered an implementation of the FFT, the Nolen matrix BFN can be considered an implementation of the discrete Fourier transform (DFT).

So, more types of beamforming networks exist. Why not use those?

- A Butler BFN generates beams, which cover the complete visible space of the array (in case of  $\frac{1}{2}\lambda$  spacing).
- As already mentioned above, the Butler BFN can be considered as an implementation of the FFT. Hence it can be expected that this BFN requires a minimum number of components. Compared to the Butler BFN in Figure 2.1, a Nolen matrix BFN would require 6 phase shifters & 6 hybrids for a 4-element array.
- A Butler BFN can be implemented using switches driven by different phases. So it is suitable for implementation in CMOS, which offers good switches.

Based on the above points, the Butler BFN is chosen in order to create multiple beams. This thesis focusses on a linear array of 4 antenna-elements (i.e.  $K = 4$ ). Therefore a 4x4 Butler matrix is analyzed. Consequently  $N = 4$ . An inter-element distance of half the wavelength (i.e.  $d = \frac{1}{2}\lambda$ ) is assumed in order to avoid *grating lobes* [Visser, 2005, §4.5.2].

## 2.4 Analysis of the Butler Matrix

In this section the mathematical representation of the Butler BFN is addressed. For clarity, Figure 2.3 visualizes the (direct) relation of the matrix with the beamforming network. Each box ( $B_{i,j}$ ) represents a phase shift corresponding to the elements of the matrix.

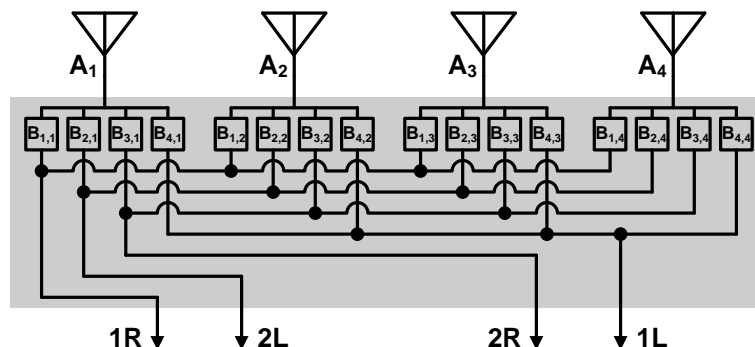


Figure 2.3: Direct implementation of the Butler matrix.

Radiation patterns, such as Figure 1.2b, are often plotted as function of the variable  $u$ . Commonly referred to as  $u$ -space. The relation of  $u$  with the angular variable  $\theta$  is described by:

$$u = \sin(\theta)$$

In array theory it is customary to describe the mathematics in  $u$ -space, since beamwidth is invariant in  $u$ -space [Visser, 2005, §7.2]. In addition, the phase term in expression (1.1) becomes linear with  $u$ .

### 2.4.1 Beam Position

In  $u$ -space, the beams of a Butler matrix are located at [Hansen, 2009, p. 346] [Mailloux, 2005, p. 392]:

$$u_i = \frac{i\lambda}{2Nd} \quad (2.2)$$

for

$$i = \pm \begin{cases} 1, 3, 5, \dots, (N-1) & \text{when } N \text{ is even} \\ 0, 2, 4, \dots, (N-1) & \text{when } N \text{ is odd} \end{cases}$$

So, in case of  $\frac{1}{2}\lambda$  spacing and a 4x4 Butler matrix, (2.2) simplifies to:

$$u_i = \frac{i}{4} \quad (2.3)$$

In u-space, the 4 beams (i.e.  $N$  is even) are located at:

$$u = \begin{cases} -0.75 & \text{when } i = -3 \\ -0.25 & \text{when } i = -1 \\ 0.25 & \text{when } i = 1 \\ 0.75 & \text{when } i = 3 \end{cases} \quad (2.4)$$

### 2.4.2 Phase Progression

The phase progression between the elements of the matrix (i.e.  $B_{i,j}$ ) is described by [Mailloux, 2005, p. 392]:

$$\delta_i = -\frac{i}{N}\pi \quad (2.5)$$

In words,  $\delta_i$  represents the increase/decrease in phase with respect to the previous row-element of the matrix. For  $N = 4$  and  $i = 1$  the phase progression becomes:

$$\delta_1 = -\frac{1}{4}\pi \quad (2.6)$$

### 2.4.3 Matrix Synthesis & Orthogonality

With the aid of (2.6), the first row of the matrix (i.e.  $B_{1,j}$ ) can be constructed. Starting from broadside direction (i.e.  $e^{j0\pi}$ ) the row-elements become:

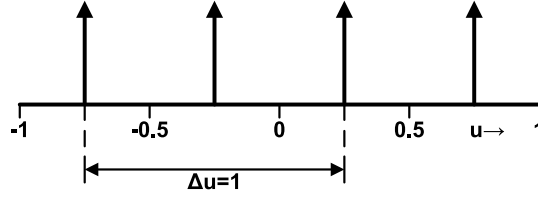
$$\left[ e^{j0\pi} \quad e^{-j\frac{1}{4}\pi} \quad e^{-j\frac{1}{2}\pi} \quad e^{-j\frac{3}{4}\pi} \right]$$

The second row of the matrix should contain the phases necessary to create a beam 'orthogonal' to the first beam (1R). Orthogonal, meaning *in geometric sense* (perpendicular).

In Figure 2.4 the beams, at the positions given by (2.4), are represented by four impulses. For  $i = 1$  expression (2.4) resulted a beam at  $u = 0.25$ . In order to be orthogonal with 1R, the second beam should be  $\pm 90^\circ$  out-of-phase with the first beam. In u-space this corresponds to:

$$u = \sin(\pm 90^\circ) = \pm 1 \quad (2.7)$$

In Figure 2.4 the result of (2.7) is indicated with  $\Delta u$ . So the first beam located at  $u = 0.25$  is orthogonal with the second beam located at  $u = -0.75$ .


 Figure 2.4: Beams located in  $u$ -space.

For  $u = -0.75$  it follows from (2.4) that  $i = -3$ . From (2.5) the phase progression for the second row of the matrix is:

$$\delta_{-3} = -\frac{-3}{4}\pi = \frac{3}{4}\pi \quad (2.8)$$

Again, starting from broadside direction, the row-elements become:

$$\left[ e^{j0\pi} \quad e^{j\frac{3}{4}\pi} \quad e^{-j\frac{1}{2}\pi} \quad e^{j\frac{1}{4}\pi} \right]$$

In a similar way the phase progression for  $i = 3$  and  $i = -1$  result the phases of the third and fourth row. Hence the Butler matrix becomes:

$$B = \begin{bmatrix} e^{j0\pi} & e^{-j\frac{1}{4}\pi} & e^{-j\frac{1}{2}\pi} & e^{-j\frac{3}{4}\pi} \\ e^{j0\pi} & e^{j\frac{3}{4}\pi} & e^{-j\frac{1}{2}\pi} & e^{j\frac{1}{4}\pi} \\ e^{j0\pi} & e^{-j\frac{3}{4}\pi} & e^{j\frac{1}{2}\pi} & e^{-j\frac{1}{4}\pi} \\ e^{j0\pi} & e^{j\frac{1}{4}\pi} & e^{j\frac{1}{2}\pi} & e^{j\frac{3}{4}\pi} \end{bmatrix} \quad (2.9)$$

The Butler beams can be calculated as:

$$\begin{bmatrix} 1R \\ 2L \\ 2R \\ 1L \end{bmatrix} = \begin{bmatrix} e^{j0\pi} & e^{-j\frac{1}{4}\pi} & e^{-j\frac{1}{2}\pi} & e^{-j\frac{3}{4}\pi} \\ e^{j0\pi} & e^{j\frac{3}{4}\pi} & e^{-j\frac{1}{2}\pi} & e^{j\frac{1}{4}\pi} \\ e^{j0\pi} & e^{-j\frac{3}{4}\pi} & e^{j\frac{1}{2}\pi} & e^{-j\frac{1}{4}\pi} \\ e^{j0\pi} & e^{j\frac{1}{4}\pi} & e^{j\frac{1}{2}\pi} & e^{j\frac{3}{4}\pi} \end{bmatrix} \begin{bmatrix} A_1 \\ A_2 \\ A_3 \\ A_4 \end{bmatrix} \quad (2.10)$$

$\mathbf{A}$  represents the element signals of the array. A multiplication with  $B$ , results the phases - apart from a rotation - as defined in (2.1).

Beams that are mutually orthogonal, are commonly referred to as *beam pairs*. In case of (2.10), these beam pairs are 1R & 2L and 2R & 1L.

## 2.5 Beam Summation

The beams generated by the Butler BFN can be summed in order to form a radiation pattern  $P(u)$ :

$$P(u) = [1 \quad 1 \quad 1 \quad 1] \begin{bmatrix} 1R \\ 2L \\ 2R \\ 1L \end{bmatrix} \quad (2.11)$$

Figure 2.5 illustrates the summing operation. The Butler BFN is represented by a black box, which could contain an implementation as illustrated in Figure 2.1.

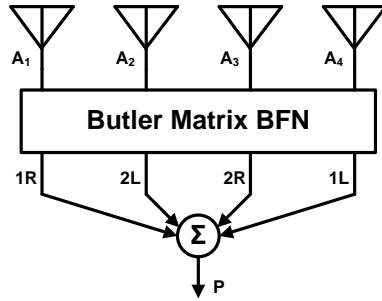


Figure 2.5: Summing the Butler beams yields the radiation pattern  $P$ .

The beams, formed by the BFN in Figure 2.1, are generated from the element signals as:

$$1R = A_1 \angle 0^\circ + A_2 \angle -45^\circ + A_3 \angle -90^\circ + A_4 \angle -135^\circ \quad (2.12a)$$

$$2L = A_1 \angle -90^\circ + A_2 \angle 45^\circ + A_3 \angle 180^\circ + A_4 \angle -45^\circ \quad (2.12b)$$

$$2R = A_1 \angle -45^\circ + A_2 \angle 180^\circ + A_3 \angle 45^\circ + A_4 \angle -90^\circ \quad (2.12c)$$

$$1L = A_1 \angle -135^\circ + A_2 \angle -90^\circ + A_3 \angle -45^\circ + A_4 \angle 0^\circ \quad (2.12d)$$

Summing these beams according to (2.11), results the radiation pattern shown in Figure 2.6a. Summing the beams, given by (2.10), yields the radiation pattern shown in Figure 2.6b. This Figure shows that different implementations of the Butler matrix represent the same Butler beams. However, when these beams are summed according to (2.11), the resulting radiation patterns ( $P$ ) differ!

The signal from one of the array elements, should always experience the same phase shift for every Butler beam. Thus, one column of the matrix should always represent the same phase shift. When the Butler matrix does not satisfy this condition, the Butler beams do not sum up to a constant value for every angle, as can be observed from Figure 2.6a. This is undesired, as will become clear from the next section.

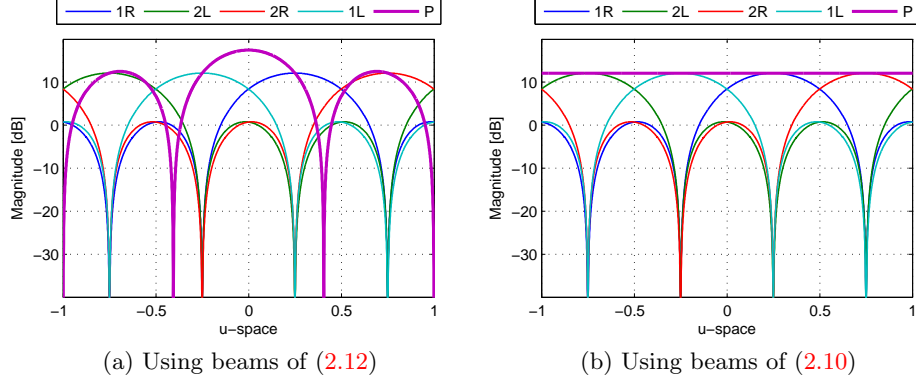


Figure 2.6: Radiation patterns of summed Butler beams.

## 2.6 Beam Cancellation

A Butler BFN distributes the received signal power of the array equally over its beam ports to form orthogonal beams. As depicted in Figure 2.2b, the angle where one of the beams is at its maximum, the other beams are zero. As an example, consider  $u = 0.25$ , where the element signals are given by:

$$\mathbf{A} = \begin{bmatrix} e^{j0\pi} \\ e^{j\frac{1}{4}\pi} \\ e^{j\frac{1}{2}\pi} \\ e^{j\frac{3}{4}\pi} \end{bmatrix} \quad (2.13)$$

At  $u = 0.25$ , beam 1R is maximal according to Figure 2.2b, as verified by this calculation:

$$\begin{aligned} 1R &= e^{j0\pi} e^{j0\pi} + e^{-j\frac{1}{4}\pi} e^{j\frac{1}{4}\pi} + e^{-j\frac{1}{2}\pi} e^{j\frac{1}{2}\pi} + e^{-j\frac{3}{4}\pi} e^{j\frac{3}{4}\pi} = 4 \\ 2L &= e^{j0\pi} e^{j0\pi} + e^{j\frac{3}{4}\pi} e^{j\frac{1}{4}\pi} + e^{-j\frac{1}{2}\pi} e^{j\frac{1}{2}\pi} + e^{j\frac{1}{4}\pi} e^{j\frac{3}{4}\pi} = 0 \\ 2R &= e^{j0\pi} e^{j0\pi} + e^{-j\frac{3}{4}\pi} e^{j\frac{1}{4}\pi} + e^{j\frac{1}{2}\pi} e^{j\frac{1}{2}\pi} + e^{-j\frac{1}{4}\pi} e^{j\frac{3}{4}\pi} = 0 \\ 1L &= e^{j0\pi} e^{j0\pi} + e^{j\frac{1}{4}\pi} e^{j\frac{1}{4}\pi} + e^{j\frac{1}{2}\pi} e^{j\frac{1}{2}\pi} + e^{j\frac{3}{4}\pi} e^{j\frac{3}{4}\pi} = 0 \end{aligned}$$

When all beams - except 1R - are summed according to (2.11), the radiation pattern ( $P$ ) contains a *null* at  $u = 0.25$ . So, if a Butler beam points into the direction of an interferer, and this beam is cancelled<sup>2</sup>, the interferer is *nulled out*. In this way the radiation pattern gets a null at the position of the cancelled beam.

<sup>2</sup>For the moment it is of no importance how this beam is actually *cancelled*.

Figure 2.7 illustrates the *principle of interference nulling* used within this work. Note that the radiation pattern in Figure 2.7b does not remain flat when a beam is cancelled. That is, the antenna gain is lowered in certain directions.

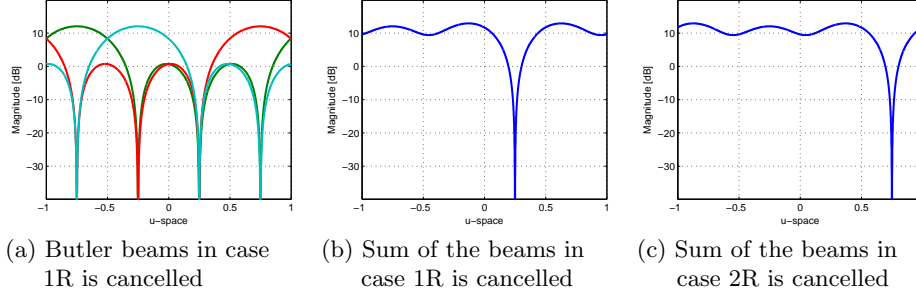


Figure 2.7: Principle of interference nulling.

The question may arise which Butler beam should be cancelled, when an interferer is present at a direction just in between two neighboring beams. Consider an interferer at  $u = 0.5$ . Which beam, i.e. 1R or 2R, should be cancelled? Figure 7.2c illustrates the case when beam 2R is cancelled. As can be seen from Figures 2.7b & 7.2c, it follows that no interferer can be nulled at  $u = 0.5$ , when either 1R or 2R is cancelled. To cancel an interferer at an arbitrary angle (i.e. from an arbitrary direction), a Butler beam should be shifted to that particular direction. This implies that all Butler beams, i.e. the whole matrix, should be shifted such that one of the beams can 'capture' the interferer.

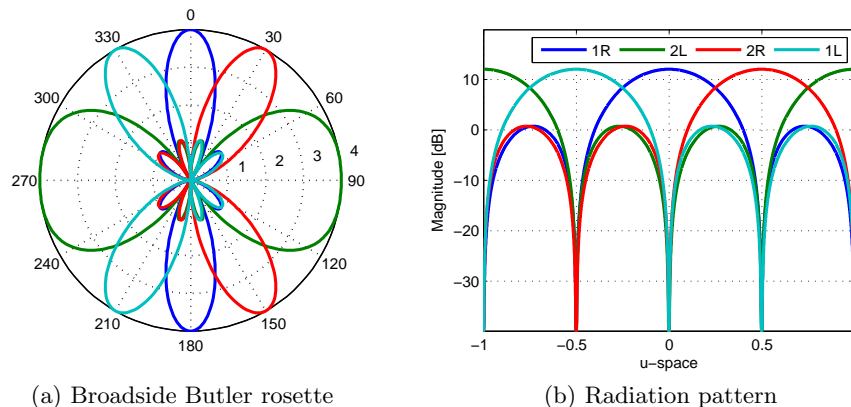
## 2.7 Broadside Butler

Expression (2.2) defines the position of Butler beams in u-space. Increasing  $i$  by 1 in (2.2) shifts the beams to:

$$u = \begin{cases} -0.5 & \text{when } i = -2 \\ 0 & \text{when } i = 0 \\ 0.5 & \text{when } i = 2 \\ 1 & \text{when } i = 4 \end{cases} \quad (2.14)$$

The beam at  $u = 1$  (i.e.  $90^\circ$ ) has a mirror beam at  $u = -1$  ( $270^\circ$ ). This can be observed from Figure 2.8.

Within this thesis, the Butler matrix that renders beams as presented in Figure 2.8, is denoted as *Broadside Butler*, because one beam points to broadside direction (i.e.  $0^\circ$ ).


 Figure 2.8: Beams of the *Broadside Butler*.

The broadside Butler matrix can be constructed in a similar way as described in section 2.4.3.

$$B_{0^\circ} = \begin{bmatrix} 0^\circ & 0^\circ & 0^\circ & 0^\circ \\ 0^\circ & 180^\circ & 0^\circ & 180^\circ \\ 0^\circ & 270^\circ & 180^\circ & 90^\circ \\ 0^\circ & 90^\circ & 180^\circ & 270^\circ \end{bmatrix} \quad (2.15)$$

Note that due to the symmetry of this matrix only 4 phases are needed. Therefore, the broadside Butler matrix can be considered as a special case of the generic Butler matrix.

As exemplified in the previous section, it was not possible to reject an interferer at  $u = 0.5$ . However, Figure 2.8 clearly shows that beam 2R (red) points at  $30^\circ$ , i.e.  $u = 0.5$ . So, using the broadside Butler matrix, the interferer located at  $u = 0.5$  can be nulled. Note that the broadside Butler matrix is in fact a shifted version of the generic Butler matrix.

*By rotating the (generic) Butler matrix such that one of its beams points into the direction of an interferer, this interferer can be nulled.*

## 2.8 Beamforming Function

In order to perform interference nulling, a Butler beam, which points into the direction of an interferer, is cancelled. In this way the interferer is nulled and the signal-to-interference ratio (SIR) is improved. Figure 2.9 presents a beamforming system which is able to perform interference nulling. The gain blocks in Figure 2.9 are used to cancel a Butler beam.

It is also desired to improve the sensitivity of the array in the direction of the signal to be received. In other words, the *beamforming function* should also improve the signal-to-noise ratio (SNR).

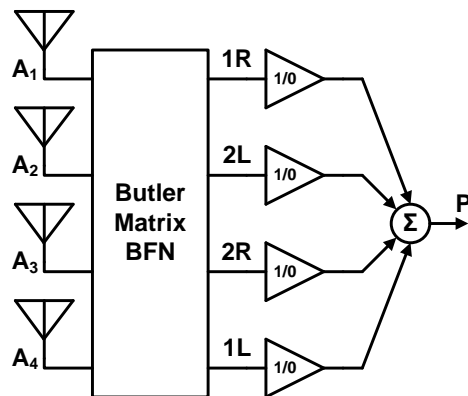


Figure 2.9: Beamforming system to perform interference nulling.

The next chapter describes a beamforming algorithm which performs interference nulling (i.e. SIR improvement) and directivity (SNR improvement).



## Chapter 3

# Beamforming Algorithm

As mentioned in section 2.8, the beamforming system should perform two functions:

1. Interference Nulling
2. Signal-to-Noise optimization

As explained in the previous chapter, interferers can be nulled by cancelling a Butler beam and summing the other Butler beams. By applying a phase shift to the other beams, such that they coherently add up, the SNR can be improved according to the principle of a phased array. In order to perform both functions, i.e. SIR & SNR optimization, a beamforming algorithm is used.

First, the complex weights, for the SIR & SNR optimized beamforming algorithm, are mathematically derived. Secondly, these complex weights are decomposed into magnitudes and phases, which are consecutive applied to the Butler beams.

### 3.1 Howells-Applebaum Algorithm

The *Howells-Applebaum* algorithm performs signal-to-noise optimization [Mailloux, 2005, p. 160]. This algorithm uses a so-called *Quiescent Steering Vector*. 'Quiescent' refers to the case that no interferers are present, such that this vector describes the complex weights, which are responsible for steering the main beam to receive some desired signal at angle  $\theta_0$ .

From Figure 1.2b it can be observed that the main beam peaks at  $\theta = 0^\circ$ . Due to the fact that  $\sin(0^\circ) = 0$ , the whole exponent in expression (1.1)

becomes zero. A certain angle of incidence gives a phase difference between the elements of the array. By phase shifting the element signals by the same - but negative - amount, the array becomes most sensitive to that direction. Therefore, to steer the main beam to a random angle, it should hold:

$$k_0(i-1)d\sin(\theta_0) = 0 \quad (3.1)$$

where  $i$  is the element number.

Defining a complex weight as:

$$\overline{w}_i = a_i e^{-j\phi} \quad (3.2)$$

Normalizing the magnitude and applying a phase shift according to (3.1):

$$\begin{aligned} a_i &= \frac{1}{K} \\ \phi &= k_0(i-1)d\sin(\theta_0) \end{aligned}$$

Such that (3.2) becomes:

$$\overline{w}_i = \frac{1}{K} e^{-jk_0(i-1)d\sin(\theta_0)} \quad (3.3)$$

When expression (3.3) is multiplied with the array factor - as defined in (1.1) - the main beam is steered to  $\theta_0$ . The radiation pattern  $P(\theta)$  becomes:

$$\begin{aligned} P(\theta) &= \sum_{i=1}^K \overline{w}_i F(\theta) \\ P(\theta) &= \sum_{i=1}^K \overline{w}_i e^{jk_0(i-1)d\sin(\theta)} \\ P(\theta) &= \sum_{i=1}^K \frac{1}{K} e^{-jk_0(i-1)d\sin(\theta_0)} e^{jk_0(K-i)d\sin(\theta)} \\ P(\theta) &= \sum_{i=1}^K \frac{1}{K} e^{jk_0(i-1)d(\sin(\theta) - \sin(\theta_0))} \end{aligned}$$

In u-space:

$$P(u) = \sum_{i=1}^K \frac{1}{K} e^{jk_0(i-1)d(u-u_0)} \quad (3.4)$$

So, the main beam peaks at  $u_0$ .

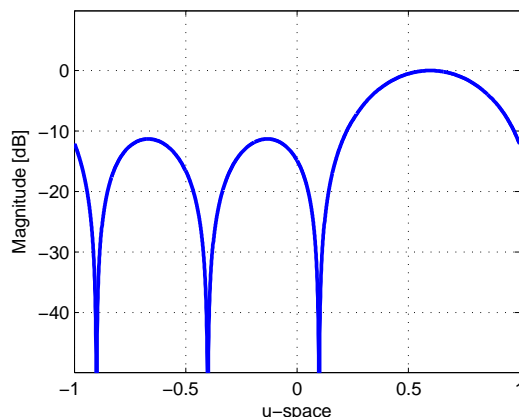


Figure 3.1: Quiescent beam pattern with main beam at  $u = 0.6$ .

When written in vector form, expression (3.3) is known as the - already mentioned - quiescent steering vector (QSV). According to the Howells-Applebaum method [Mailloux, 2005, p. 163], the SIR is maximized by using complex weights to move one of the natural pattern nulls to the position of the interferer. This principle can be forced by subtracting a so-called *cancellation pattern* from the *quiescent beam pattern* (i.e. the radiation pattern where the main beam is steered to receive some desired signal at angle  $\theta_0$ ).

Figure 3.1 illustrates the quiescent beam pattern as a result of applying the QSV for  $u_0 = 0.6$ .

## 3.2 Synthesis of the Complex Weights

The quiescent beam pattern is the result of applying complex weights (i.e. the QSV) to the array factor as presented by expression (3.4). In a similar way a cancellation pattern can be synthesized. The cancellation pattern is defined as the radiation pattern where the main beam is steered to the position of the interferer. In order to force a null, the cancellation pattern is normalized to the level of the side lobes of the quiescent beam pattern at the position of the interferer. Subsequently, the (normalized) complex weights for the cancellation pattern are subtracted from the QSV. In this way the complex weights for the *interference nulled radiation pattern* are determined.

Summarizing the above described procedure:

1. Next to the quiescent beam pattern, a second radiation pattern is used with the main beam steered to the position of the interferer, such that  $u_0 = u_{int}$ . This pattern is defined as the cancellation pattern.

2. The cancellation pattern is normalized to the quiescent beam pattern at the interferer position ( $u_{int}$ ).
3. The complex weights of the normalized cancellation pattern are subtracted from the QSV. The resulting complex weights render the interference nulled radiation pattern, such that interference nulling is performed.

Figure 3.2 illustrates the principle for an interferer at  $u = -0.7$ .

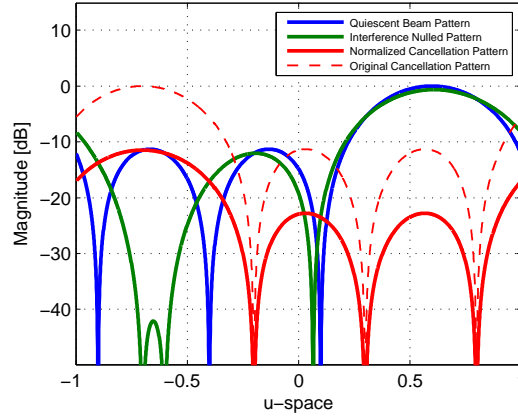


Figure 3.2: Synthesis of the interference nulled radiation pattern (in green). Main beam steered to  $u = 0.6$ . Null created at  $u = -0.7$ .

Defining the *Interference Steering Vector* (ISV), being the complex weights for the cancellation pattern and the QSV as:

$$\mathbf{QSV} = \frac{1}{K} e^{-jk_0 M d u_0}$$

$$\mathbf{ISV} = \frac{1}{K} e^{-jk_0 M d u_{int}}$$

where

$$\mathbf{M} = [0 \quad 1 \quad 2 \quad (K - 1)]^T$$

In order to normalize the cancellation pattern to the level of the side lobes of the quiescent beam pattern (as depicted in Figure 3.2), the **ISV** should be normalized. That is, the complex value of the cancellation pattern should become equal to the complex value of the quiescent beam pattern at the position of the interferer, i.e.  $P(u_{int})$ . When both patterns are equal at the position of the interferer and their complex weights (i.e. **QSV** & **ISV**) are subtracted from each other, a null is created.

The complex weight, as defined by expression (3.3), already normalizes the magnitude of the radiation pattern, such that the main beam peaks to 0 dB

(i.e. 1). This is convenient in order to obtain the same complex value for both patterns at the interferer position. The quiescent beam pattern, evaluated at the position of the interferer ( $u_{int}$ ) is:

$$P(u_{int}) = \sum_{i=1}^K \frac{1}{K} e^{jk_0(i-1)d(u_{int}-u_0)} \quad (3.5)$$

Thus  $P(u_{int})$  provides the normalization factor, such that the complex weights ( $\mathbf{W}$ ) for the interference nulled radiation pattern become:

$$\mathbf{W} = \mathbf{QSV} - P(u_{int})\mathbf{ISV} \quad (3.6)$$

As a result, the interference nulled radiation pattern becomes:

$$P(u) = \sum_{i=1}^K W_i e^{jk_0(i-1)du} \quad (3.7)$$

The interference nulled beamforming algorithm performs SNR optimization by steering the main beam to the direction where the wanted signal is to be received and performs SIR optimization by forcing a null via a subtraction of complex weights.

### 3.3 2-Step Beamforming

In Chapter 2 is described how interference nulling is performed by cancelling a Butler beam. The previous section described a beamforming algorithm which also performs interference nulling. What is the relation between the *principle of interference nulling* as defined in Chapter 2 and the above described beamforming algorithm?

The principle of interference nulling only gives SIR optimization, while the previously discussed beamforming algorithm performs both SIR and SNR optimization. Consequently, beam cancellation can be considered a subset (i.e. only SIR optimization) of the beamforming algorithm. However, the principle of beam cancellation can be used for *beam weighting*. When the Butler beams are weighted, the magnitudes of the complex weights - as determined by the algorithm (see section 3.2) - can be synthesized.

#### 3.3.1 Beam Weighting

In order to obtain the *magnitude weights* for the Butler beams, these weights have to be solved, using:

1. The Butler matrix.
2. The complex weights determined by the algorithm, i.e.  $\mathbf{W}$  (3.6).

That is, a system of linear equations has to be solved. According to (3.7), the *wanted* interference nulled radiation pattern is:

$$P(u) = \sum_{i=1}^K W_i A_i \quad (3.8)$$

where

$$A_i = e^{jk_0(i-1)du}$$

So, in order to synthesize the magnitudes of  $\mathbf{W}$ , the Butler beams have to be weighted. Defining a column vector  $\mathbf{C}$  and using expression (2.10), the *wanted* interference nulled radiation pattern can be written as:

$$P(u) = \mathbf{C}^T \begin{bmatrix} 1R \\ 2L \\ 2R \\ 1L \end{bmatrix} \quad (3.9)$$

Equating expressions (3.8) & (3.9), such that the pattern to be synthesized with weighted Butler beams equals the wanted pattern:

$$\mathbf{C}^T \begin{bmatrix} 1R \\ 2L \\ 2R \\ 1L \end{bmatrix} = (\mathbf{W}^*)^T \mathbf{A} \quad (3.10)$$

Recall that the Butler beams are the result of multiplying the Butler matrix ( $B$ ) with the element signals ( $\mathbf{A}$ ), as derived at (2.10):

$$\mathbf{C}^T B \mathbf{A} = (\mathbf{W}^*)^T \mathbf{A} \quad (3.11)$$

$$\mathbf{C}^T B = (\mathbf{W}^*)^T \quad (3.12)$$

In expression (3.12) a matrix equation of the form  $\mathbf{A}\mathbf{x}=\mathbf{b}$  may be recognized. From (3.12), the solution vector  $\mathbf{C}$  can be solved:

$$\mathbf{C}^T = (\mathbf{W}^*)^T B^{-1} \quad (3.13)$$

Expression (3.13) defines the complex weights for the Butler beams, of which the magnitudes are:

$$a_i = |C_i| = \sqrt{\Re(C_i)^2 + \Im(C_i)^2} \quad (3.14)$$

When the Butler beams are shifted (i.e. rotating the matrix), such that one of the beams points into the direction of an interferer, one element of  $|\mathbf{C}|$  is always zero. Consequently the Butler beam is cancelled and thus the interferer, just like the principle of interference nulling as introduced in Chapter 2.

Solving the linear system as presented by (3.12), not only results the weighted magnitudes for the Butler beams, but a whole new set of complex weights. Consequently, also phase shifts are introduced. This implies a new system function, i.e. *phase shifting*.

### 3.3.2 SNR Optimization

According to equation (3.12), a phase shifting function should be added to the beamforming system in order to synthesize the complex weights ( $\mathbf{C}$ ) using orthogonal (i.e. Butler) beams.

$$\varphi_i = \arg(C_i) = \arctan\left(\frac{\Im(C_i)}{\Re(C_i)}\right) \quad (3.15)$$

Therefore, beamforming is performed in two steps. In the first step the Butler matrix is rotated such that one of the beams captures an interferer. When the beams are weighted according to expression (3.14), interference nulling is performed.

The function of the second step is to improve the SNR. This is achieved by phase shifting the Butler beams in a way that they coherently add up, just like the principle operation of a phased array. Figure 3.3 illustrates the total interference nulled beamforming system.

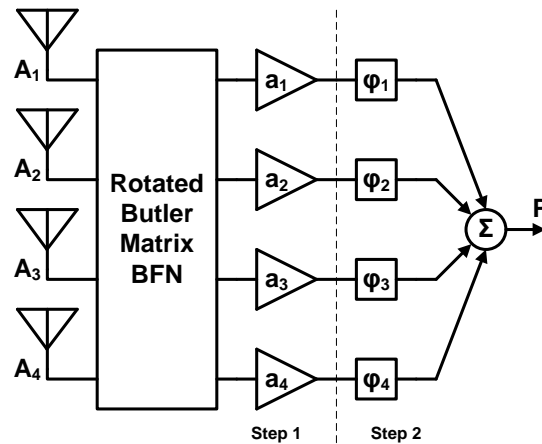


Figure 3.3: 2-step interference nulled beamforming system.

When the complex weights of the Butler matrix ( $e^{j\phi}$ ) and the magnitude weights ( $a_i$ ) are quantized (i.e. limited in resolution), the phase shifters also improve the SIR. In contrast to a phased array, the proposed beamforming system in Figure 3.3 performs interference nulling prior to the phase shifters. In this way the nulling requirements, in terms of resolution, for the phase shifters are relaxed. So the phase shifters not only perform SNR optimization, but also SIR optimization.

## Chapter 4

# Beamforming Platform

In this chapter the functions of the beamforming system are reviewed. In addition, an existing platform is introduced which is suitable for implementing the beamforming system.

### 4.1 System Functions

As illustrated in Figure 3.3, the radiation pattern of the proposed beamforming system can be written as:

$$P(\theta) = \sum_{i=1}^K a_i e^{j\varphi_i} B \cdot A_i(\theta) \quad (4.1)$$

As becomes clear from expression (4.1), the elements of the beamforming system are easily recognized:

- Butler matrix  $B$
- Magnitude weights  $a$ , i.e.  $|\mathbf{C}|$
- Phase weights  $\varphi$ , i.e.  $\arg(\mathbf{C})$
- Summation of the antenna signals

As exemplified in section 1.4, a phase-shifting function - which is typical for a phased array - by means of a vector modulator, can be implemented via a combination of resistors and an Op-Amp. Thus, *the complex weights of a phased array can be implemented using resistors and Op-Amps*. However, the magnitude weights should also be implemented using a combination of Op-Amps & resistors.

Part of this work is to examine if the above listed functionalities can be implemented in a similar way. In other words:

*How can these functions be mapped to a circuit level implementation?*

Apart from a single antenna input, the receiver - as reported in [Ru et al., 2009] - provides the hardware for a potential implementation, and thus can serve as a platform for the proposed beamforming system. This front-end is shown in Figure 4.1.

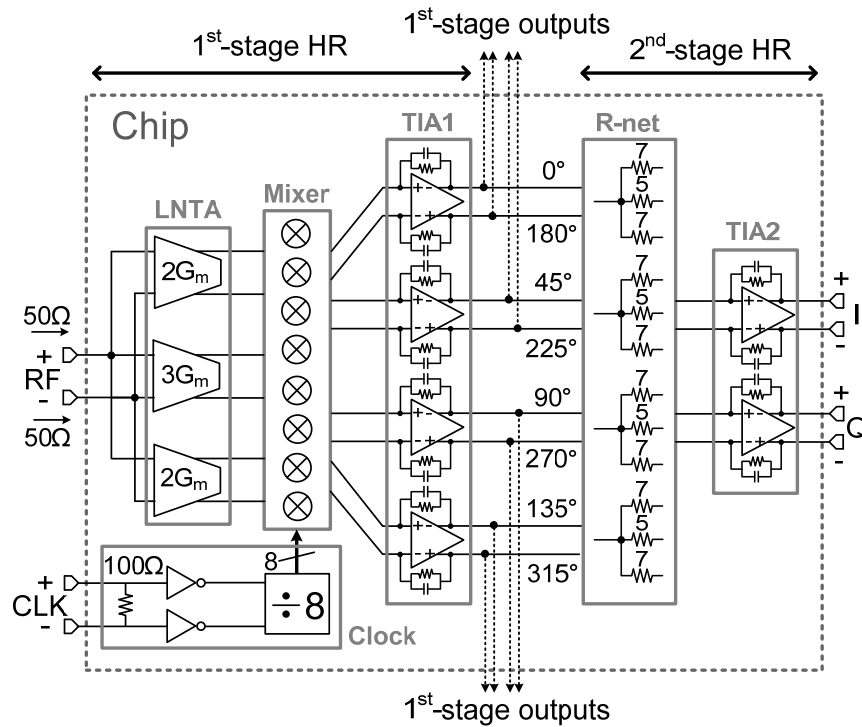


Figure 4.1: Software defined radio receiver as reported in [Ru et al., 2009].

## 4.2 Motivation

The main features of this front-end for beamforming purposes are:

- Low-noise transimpedance amplifier (LNTA), providing  $50\ \Omega$  input impedance and  $V \rightarrow I$  conversion
- 8-phase passive mixer
- 2 transimpedance amplifier (TIA) stages
- High linearity

### 4.2.1 Mixer Array

The passive mixer array is driven by an 8-phase local oscillator (LO). The passive mixer simply consists of NMOS switches, which perform the frequency translation. In a similar way, i.e. using switches, a Butler BFN can be constructed. Since the LO provides 8 phases, different mixer outputs can be combined to form a Butler beam (in case of multiple antennas). Since the mixer operates in the current domain, the down-converted & phase-shifted signals from multiple antenna-elements are easily summed to form a Butler beam.

### 4.2.2 TIA Stages

Both Op-Amp stages are configured as a transimpedance amplifier (TIA) via resistive feedback. The transimpedance is largely defined by the feedback resistor. The R-net in between the TIA stages serves as a weighting network for harmonic rejection (HR).

#### TIA1

In the proposed platform, the first TIA stage is driven by the down-converted LNTA current. When the transimpedance is programmable, the output voltage (1<sup>st</sup>-stage outputs in Figure 4.1) can be adjusted. In this way a Butler beam can be attenuated by lowering the transimpedance. Thus the first TIA stage can be extended as implementation for the magnitude weights ( $a$ ) of the beamforming system.

#### TIA2

The second TIA stage performs the weighted summation of currents via a resistor network (R-net in Figure 4.1). As introduced in Chapter 3, a phase shifter is required in order to improve the SNR of the beamforming system. In other words, a phase shifting function is needed to cohere the antenna signals. When these synchronized signals sum up, the SNR is improved. Since differential in-phase (I) and quadrature (Q) signals are present at the input of TIA2, a phase shifter can be constructed by means of a vector modulator. In this way the phase weights ( $\varphi$ ) of the beamforming system can be implemented. In addition, the antenna signals can be summed to generate the radiation pattern ( $P$ ).

### 4.2.3 Linearity

As becomes clear in the above sections, this architecture is well suited for implementation of the system functions, i.e. the proposed beamforming system. However, the most important feature of this receiver - in the context of beamforming - is *high linearity*.

Especially this property fits the main goal of this work, namely interference nulling. Because of high linearity, this front-end is highly tolerant to strong interferers. In order to prevent clipping to the supply (which is very limited in modern CMOS processes) voltage gain is avoided at RF. Consequently, these blockers can be processed in the current domain from RF to IF and subsequently be suppressed at the first TIA stage where voltage gain occurs.

Figure 4.2 presents the proposed beamforming system, utilizing the features of the above described front-end. In Figure 4.2,  $n$  represents the number of phase-shifted mixer outputs, which are summed in the summation network to form a Butler beam.

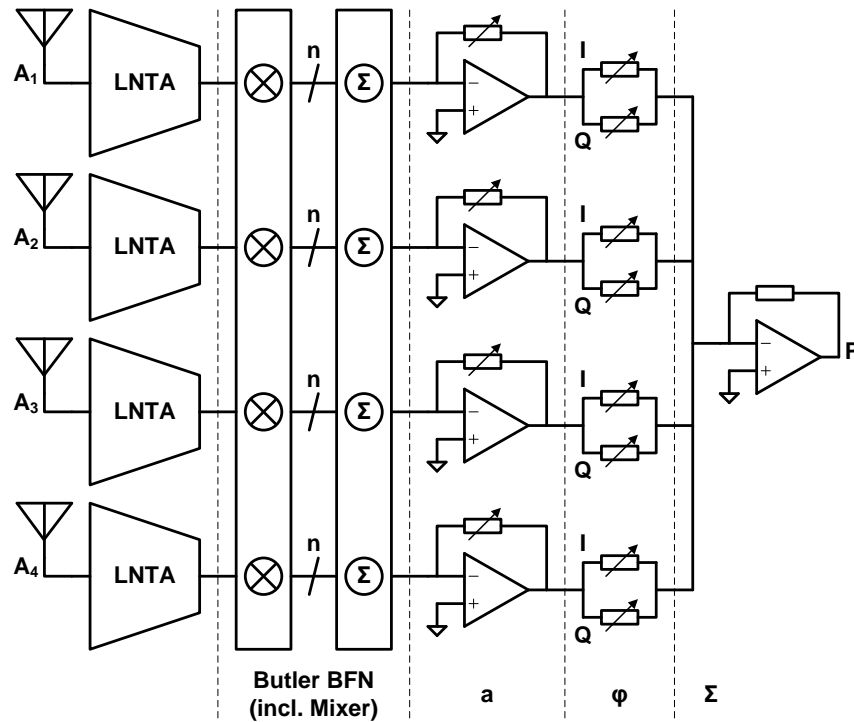


Figure 4.2: Beamforming system mapped onto the platform.

## Chapter 5

# System Model Evaluation

The previous chapter described a receiver front-end, suitable for implementation of the proposed beamforming system. This chapter evaluates the performance of the beamforming system, subject to constraints imposed by a circuit implementation. In order to model the circuit implementation as shown in Figure 4.2, the complex weights of the proposed beamforming system are quantized. In this chapter, simulations of the system model with quantized weights are presented. It will become clear that a circuit implementation imposes constraints to the system performance.

### 5.1 Circuit Constraints

The proposed platform described in Chapter 4 imposes constraints, which limit the performance. This section addresses these limitations with respect to the (ideal) system design.

#### 5.1.1 Butler Beamforming Network

The proposed front-end provides an 8-phase LO ( $\frac{1}{8}$  duty-cycle clock) for down conversion. These phases can also be used for the Butler BFN. Switches, driven by different LO phases, can be used to perform phase shifting. More phases enables more possible Butler matrix implementations and hence better null steering (as explained in Chapter 2). However, dividing the master clock signal (CLK in Figure 4.1) into more phases (e.g. 16), will result a lower LO frequency. In that case, RF signals cannot be down converted to baseband anymore. Therefore a maximum of 8 phases can be used for the Butler BFN.

### 5.1.2 Weight Quantization

The complex weights ( $\mathbf{C}$ ), as determined by the beamforming algorithm (see section 3.3), should be implemented using resistors. A variable resistance can only have a finite number of values. Thus, the complex weights (i.e. resistors) should be quantized. Keeping a circuit implementation in mind, realistic quantization levels are chosen. The beamforming algorithm results magnitude weights ( $a_q$ ) normalized between 0 and 1 and phase weights ( $\varphi_q$ ) normalized between  $0^\circ$  and  $360^\circ$ . Expressing the number of quantization levels in bits ( $b$ ) results:

$$a_q = \frac{q - 1}{2^b - 1} \quad (5.1)$$

$$\varphi_q = \frac{q - 0.5}{2^b} 360^\circ \quad (5.2)$$

where

$$1 \leq q \leq 2^b$$

Consider a phasor diagram with a phasor at  $0^\circ$  in the first quadrant and a phasor at  $90^\circ$  in the fourth quadrant. These vectors overlap. Therefore,  $\varphi_q$  has an  $\frac{1}{2}$  LSB offset from the I/Q axis.

## 5.2 Model Simulations

The interference nulled radiation pattern ( $P$ ) is evaluated for various quantization settings. Figures 5.1 - 5.3 present benchmark curves, to identify the performance of the beamforming algorithm. In each figure, the main beam is steered to  $u = 0.6$ <sup>1</sup>, while the position of an interferer is swept from  $u = -1$  (endfire) to  $u = 0.5$ , i.e.  $30^\circ$ . The blue curves represent the magnitude of one of the Butler beams, which is maximal at the position of the interferer. This curve can be considered the nulling performance of the first stage in Figure 4.2. The green curves represent the total nulling performance, so including phase shifting and beam summation. The red curves represent the level of the main beam. All curves are relative to 0 dB.

### 5.2.1 Quantized Butler Phases

Figure 5.1 presents the nulling performance of the beamforming algorithm as a result of constructing the Butler matrix with a limited number of LO

<sup>1</sup>This value is chosen because, for low resolutions (i.e. strong quantization), a Butler beam does not point to  $u = 0.6$

phases. The Butler phases are quantized to 2, 3 & 4 bits. In this way a *rotational broadside Butler* (i.e. using 4 LO phases) and a rotational standard Butler (using 8/16 LO phases) can be constructed. The algorithm rotates the Butler matrix such that one of the beams captures the interferer. The magnitude weights (i.e.  $a_q$ ) and the phase weights (i.e.  $\varphi_q$ ) are both quantized to 5 bit.

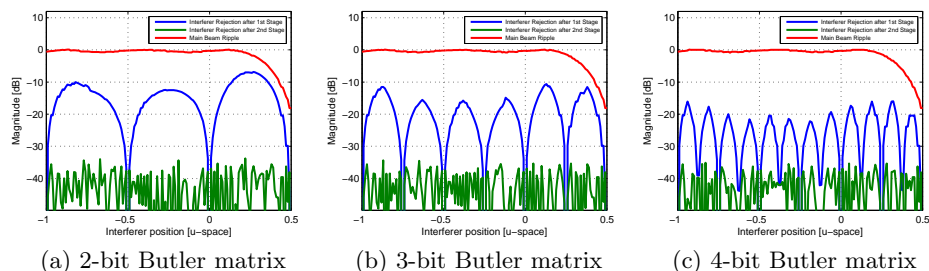


Figure 5.1: 2-stage nulling performance due to quantized Butler phases.

As mentioned above, the blue curve represents the nulling performance of the first stage. More bits, i.e. more phases, means that a Butler beam can be steered more accurately into the direction of the interferer. Figure 5.1 clearly shows that more Butler phases result more nulls (see the blue dips), which are located at the positions of the Butler beams (see Figure 2.4). The green curve shows a large rejection for each scenario, due to the relatively high resolution (5 bit quantization) of  $a_q$  &  $\varphi_q$ . The red curve is ideally 0 dB, but shows some variation due to overall quantization. When the interferer approaches the main beam at  $u = 0.6$ , the red curve falls off.

Simulations of the system model result the (minimum) interference rejection figures and the main beam loss for each quantization level. Table 5.1 presents these figures, which apply to the interval  $u = [-1 \dots 0.1]$ , since from  $u = 0.1$  the red curve starts to fall off because the interferer approaches the main beam.

Number of quantization bits	2 bit	3 bit	4 bit
First stage rejection [dB]	-10.07	-11.53	-16.04
Second stage rejection [dB]	-34.02	-34.39	-35.10
Main beam loss [dB]	-0.80	-0.85	-0.86

Table 5.1: Minimum rejection values due to quantized Butler phases.

### 5.2.2 Quantized Magnitude Weights

In a similar way, as described in the previous section, the effect of quantizing the magnitude weights ( $a_q$ ) is evaluated. Figure 5.2 presents the nulling performance of the beamforming algorithm for various quantization levels. The Butler phases are quantized to 3 bit (i.e. 8 phases) and 5 bit quantization is used for the phase weights.

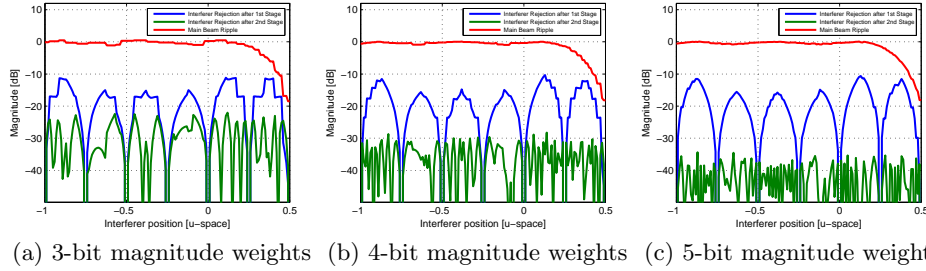


Figure 5.2: 2-stage nulling performance due to quantized magnitude weights.

The blue curves, i.e. first stage rejection, remain relatively constant. However, more bits result smoother curves due to finer quantization steps. The total interference rejection (green curves) improves with approximately 6 dB for each bit that is added. The ripple of the red curve becomes smaller for each bit that is added.

Table 5.2 presents the (minimum) interference rejection figures and the main beam loss for each quantization level. Again, the presented values in Table 5.2 apply to the interval  $u = [-1 \dots 0.1]$ .

Number of quantization bits	3 bit	4 bit	5 bit
First stage rejection [dB]	-11.32	-11.57	-11.53
Second stage rejection [dB]	-22.39	-28.67	-34.39
Main beam loss [dB]	-1.10	-0.93	-0.85

Table 5.2: Minimum rejection values due to quantized magnitude weights.

### 5.2.3 Quantized Phase Weights

Finally, the quantization of the phase weights ( $\varphi_q$ ) is examined. Figure 5.3 presents the nulling performance. Both Butler phases and magnitude weights are quantized to 3 bit.

The blue curves remain equal, while the green curves lower with approximately 6 dB for each bit that is added. Due to the interference nulling in the

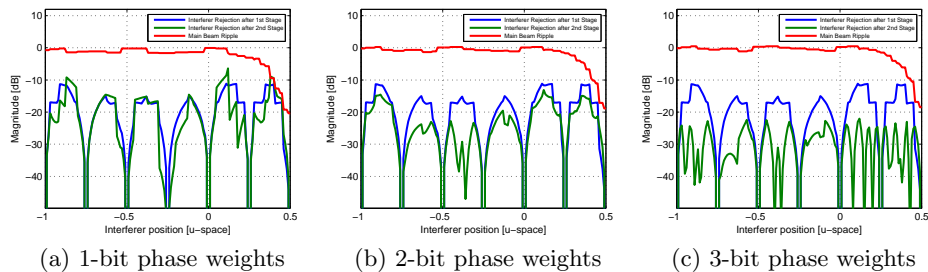


Figure 5.3: 2-stage nulling performance due to quantized phase weights.

first stage, the (quantization) requirements for the phase weights (i.e. the vector modulator) are heavily relaxed. Therefore, using more bits, does not result better nulling performance. The ripple of the main beam is smoothed, in case more bits are used.

Table 5.3 presents the (minimum) interference rejection figures and the main beam loss for each quantization level. Once again, the values in Table 5.3 apply to the interval  $u = [-1 \dots 0.1]$ .

Number of quantization bits	1 bit	2 bit	3 bit
First stage rejection [dB]	-11.32	-11.32	-11.32
Second stage rejection [dB]	-9.14	-14.58	-22.39
Main beam loss [dB]	-1.63	-1.36	-1.10

Table 5.3: Minimum rejection values due to quantized phase weights.



## Chapter 6

# Circuit Level Design

In this chapter, circuits are proposed to implement the beamforming system. As addressed in Chapter 5, a circuit implementation imposes constraints, in terms of performance, compared to the ideal system model. These constraints (i.e. quantization) serve as specification for the circuit implementation. These *circuit specifications* are:

- Maximal 8 LO phases for synthesizing the Butler BFN.
- 3-bit linear transimpedance setting in the first TIA stage.
- 5-bit uniform phase setting in the second TIA stage.

### 6.1 Beamforming Front-End

In Figure 6.1, a four-element linear array feeds the front-end, which accommodates four signal paths. Each path consists of a low-noise transconductance amplifier (LNTA), providing  $50\ \Omega$  input impedance and  $V \rightarrow I$  conversion. Subsequently, a passive mixer array, operating in the current domain, performs frequency translation. Each transconductance block consists of four small LNTAs, driving the mixer blocks. At IF, a summation network constructs four Butler beams. The passive mixer array together with the summation network, implement the Butler BFN.

The first TIA stage, with programmable transimpedance, implements the magnitude weights ( $a_q$ ), weighting the Butler beams and performing  $I \rightarrow V$  conversion. Next, a programmable resistor network (weighting in-phase & quadrature versions of each signal such that phase shifting is performed) together with a second TIA stage (summing the antenna signals and performing  $I \rightarrow V$  conversion) forms a vector modulator.

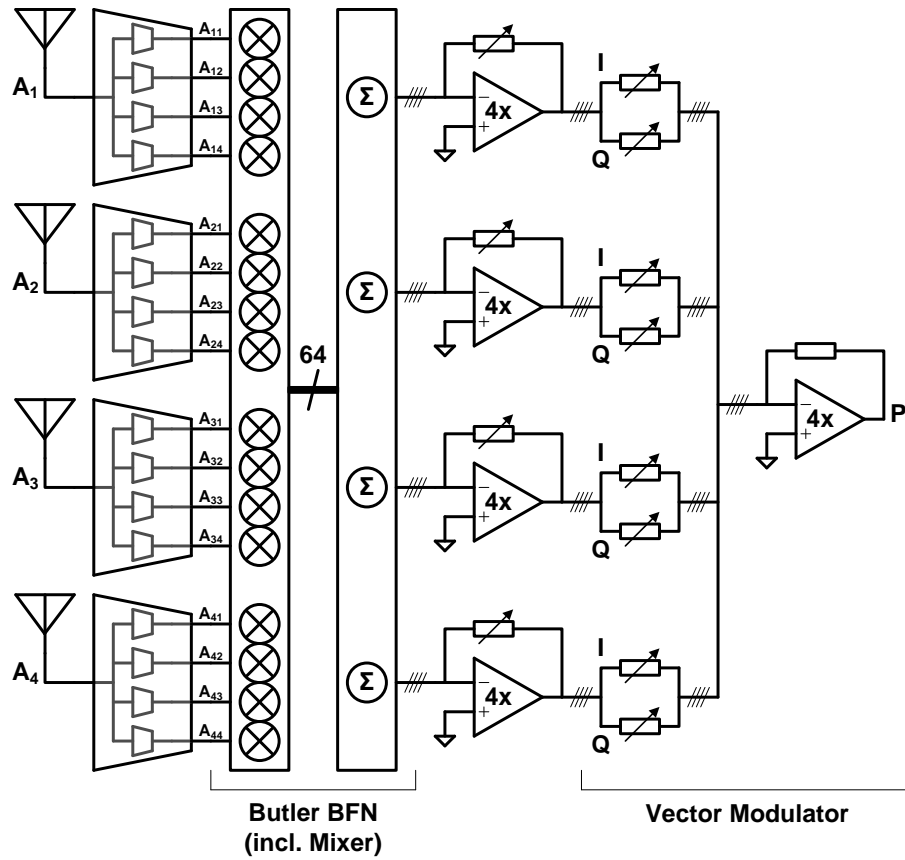


Figure 6.1: Front-end based on [Ru et al., 2009] suitable for beamforming.

Figure 6.1 shows the proposed beamforming system using 4 LO phases, such that a broadside Butler BFN can be implemented. In a similar way an 8-phase system can be constructed, using 8 signal paths. However, on behalf of circuit complexity and to save simulation time, a 4-phase system is actually implemented and simulated, in order to verify the functional operation. Therefore, the following sections apply to the '4-phase version' of the proposed beamforming system.

## 6.2 Mixer Block

The passive mixer array in Figure 6.1 consists of 16 mixer blocks. Figure 6.2 shows such a mixer block, which is used on behalf of down conversion. Each mixer block is driven by a separate LNTA (which has a high output impedance), in order to prevent current flowing back, via the Butler BFN, to other virtual grounds of the Op-Amps in the first TIA stage.

In case these mixer blocks would not be driven by separate LNTAs, an undefined current distribution between the virtual grounds of the first TIA stage would occur, leading to a pre-weighting of the Butler beams, which is unwanted. In addition, noise & offset problems can arise.

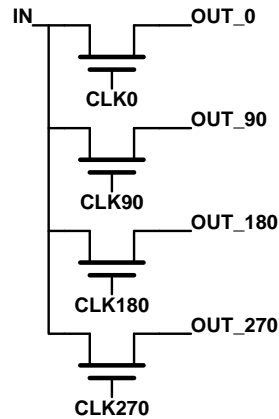


Figure 6.2: Passive down-conversion mixer.

Note that the phases for the Butler BFN are generated in these mixer blocks.

### 6.3 Butler BFN

A Butler beamformer is implemented as shown in Figure 6.3. Four of these configurations, implement the whole Butler BFN.

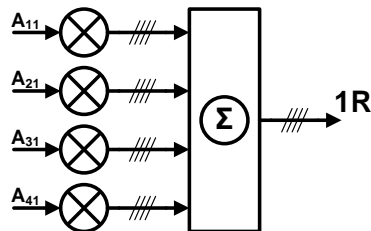


Figure 6.3: Implementation of a Butler beamformer.

As mentioned before, the LNTAs, driving the mixer blocks, prevent current flowing back to other virtual grounds.



### 6.4.2 Transimpedance

RF input power typically ranges from -40 to -30 dBm. However, according to [Ru et al., 2009], in-band interference can be as strong as -30 to -20 dBm. Consider an in-band interferer of -20 dBm, i.e. 10  $\mu$ W input power. Since the LNTA stage performs a transconductance of 20 mS, i.e. 50  $\Omega$  transimpedance, it can be derived what the maximum transimpedance for the first TIA should be, in order to prevent clipping to the supply.

According to  $P = \frac{V^2}{R}$ , 10  $\mu$ W input power results an rms voltage of approximately 22.36 mV when dissipated in a resistor of 50  $\Omega$ . Assuming a sinusoidal input signal, this corresponds to an amplitude of 31.62 mV. Consequently 20  $\times$  voltage gain (i.e.  $V_{TOP} = 632$  mV) can clip an in-band interferer of -20 dBm to a 1.2 V supply, when biased at  $\frac{1}{2}V_{DD}$  (i.e.  $V_{CM} = 600$  mV).

### 6.4.3 MOST Switches

When an NMOS transistor operates in triode region, its drain current is [Razavi, 2001, p. 17]:

$$I_D = \mu_n C_{ox} \frac{W}{L} \left[ (V_{GS} - V_{TH})V_{DS} - \frac{1}{2}V_{DS}^2 \right] \quad (6.1)$$

To let a MOS transistor operate as a switch, the device must be in deep triode region. That is  $V_{DS} \ll 2(V_{GS} - V_{TH})$ . Hence the quadratic term in (6.1) can be neglected, so (6.1) becomes:

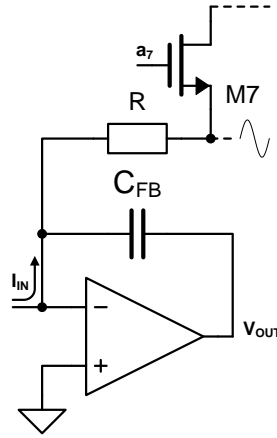
$$I_D \approx \mu_n C_{ox} \frac{W}{L} [(V_{GS} - V_{TH})V_{DS}] \quad (6.2)$$

The drain current has become a linear function of the drain-source voltage, hence the transistor operates as a linear resistor. Writing  $R_{on} = \frac{I_D}{V_{DS}}$  results:

$$R_{on} = \frac{1}{\mu_n C_{ox} \frac{W}{L} (V_{GS} - V_{TH})} \quad (6.3)$$

An ideal switch has an *on-resistance* ( $R_{on}$ ) of 0  $\Omega$ . To operate as a switch, a MOS transistor should have an  $R_{on}$  as small as possible. According to (6.3), a low on-resistance can be obtained by increasing the width of the transistor ( $W$ ) or increasing the gate-source voltage ( $V_{GS}$ ). In practice, both parameters are used to lower  $R_{on}$ .

Furthermore it is desired to keep  $R_{on}$  constant. Note the position of the switches, i.e. M0-M7, in Figure 6.4. Consider Figure 6.5 where the positions of a resistor and an NMOST are interchanged.

Figure 6.5: Voltage swing modulating  $R_{on}$ .

The input current ( $I_{IN}$ ) causes voltage swing at the source of M1, due to the resistor. Consequently the gate-source voltage of M1 is modulated according to  $I_{IN}$ . Thereby changing  $R_{on}$  and hence introducing nonlinearity. In Figure 6.4 all NMOSTs have their source tied at the inverting input of the Op-Amp, i.e. virtual ground. In this way the gate-source voltage is relative constant and thus  $R_{on}$  remains relatively constant.

#### 6.4.4 Charge Pump

In order to obtain a relatively low  $R_{on}$  compared to the total feedback resistance, a high gate-source voltage is desired. Since the common-mode level is half  $V_{DD}$ , i.e.  $V_{CM} = 600$  mV, the gate-source voltage is limited to:

$$V_{GS} = V_{DD} - V_{CM} = 1.2 - 0.6 = 600 \text{ mV}$$

The used NMOS transistors have a threshold voltage ( $V_{TH}$ ) of 415 mV. Consequently, the maximum overdrive ( $V_{GS} - V_{TH}$ ) is 185 mV, which is too low for  $R_{on}$ . Therefore, a voltage higher than  $V_{DD}$  is necessary in order to obtain a sufficiently low  $R_{on}$ . A common solution is to employ a charge pump, which can generate a voltage higher than the supply from which it is operating. A useful introduction is given by [Pylarinos].

Figure 6.6 presents a charge pump. Note that this thesis does not focus on charge-pump design. However, an example is presented to illustrate that such a circuit can be used in order to obtain voltages well above the supply.

When  $V_{CLK}$  goes low (i.e. 0 V), point A is grounded such that C1 is charged to  $V_{DD} - V_{TH}$ . When  $V_{CLK}$  goes high (i.e.  $V_{DD}$ ), the gates of M2 & M3

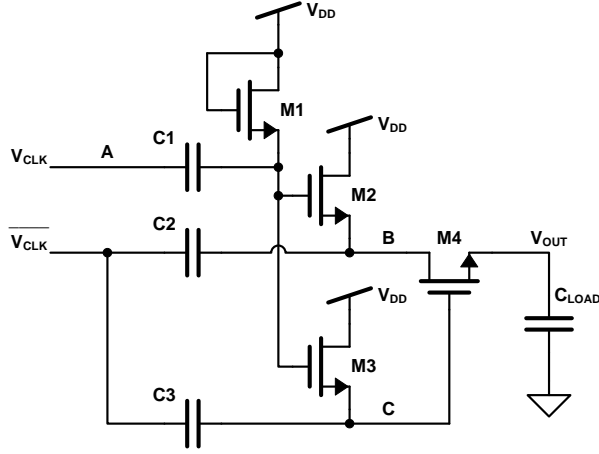


Figure 6.6: Charge pump from [Baker, 2010, §18.4.1].

sense a voltage of:

$$V_{DD} + V_{C1} = V_{DD} + (V_{DD} - V_{TH}) = 2V_{DD} - V_{TH}$$

This causes M2 & M3 to turn on, so that points B & C are pulled to  $V_{DD}$ . When  $V_{CLK}$  returns back to zero (i.e.  $\overline{V_{CLK}} \Rightarrow V_{DD}$ ), the sources of M2 & M3 swing up to  $2V_{DD}$ , such that  $C_{LOAD}$  is charged to  $2V_{DD} - V_{TH}$ .

The output voltage reaches 1.77 V with a 1.4 mV ripple using minimum sized transistors and a load capacitor of 150 fF. Due to non-idealities, the simulated output voltage is 215 mV lower than the theoretical value.

### 6.4.5 Bandwidth

The bandwidth of the first TIA stage is limited to 20 MHz. This should be sufficient in order to accommodate most mobile communication standards [Ru et al., 2009, §5.4.4]. The feedback capacitor ( $C_{FB}$ ) limits the bandwidth for a fixed resistance according to:

$$B_{-3\text{dB}} = \frac{1}{2\pi RC_{FB}} \quad (6.4)$$

## 6.5 Vector Modulator

As concluded in section 3.3.1, a phase shift function is required for the beamforming system. The proposed platform provides differential in-phase (I) and quadrature (Q) signals, so that the phase shifter can be implemented as a vector modulator (as introduced in section 1.4).

### 6.5.1 Vector Modulation

Figure 6.7 presents a phasor diagram, in order to illustrate the phase shifting function by means of *vector modulation*. A phasor (or *phase vector*) can be defined as the sum of a horizontal component (i.e. vector I) and a vertical component (vector Q). In Figure 6.7, the lengths of these I & Q vectors are linearly modulated via uniform steps (denoted by  $\Delta L$ ). The I/Q vectors are complementary in length, so when vector I increases by  $\Delta L$ , vector Q decreases by  $\Delta L$  and vice versa.

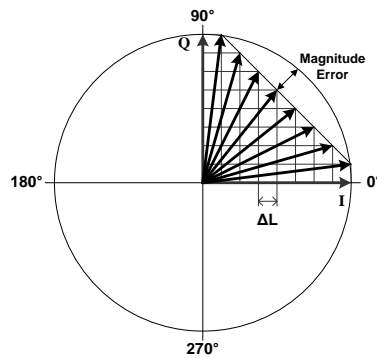


Figure 6.7: Phasor Diagram with linear modulated I & Q vectors.

As becomes clear from Figure 6.7, using uniform steps (i.e. weights) for the I & Q vectors, results into a magnitude error (i.e. a deviation from the unit circle). This error is undesired, since the contributions of each signal path in the front-end of Figure 6.1 need to be properly summed, in order to render the correct radiation pattern. Figure 6.8 presents a phasor diagram illustrating a *proper* vector modulator function, which is described by Euler's formula:

$$e^{j\varphi} = \cos(\varphi) + j \sin(\varphi) \quad (6.5)$$

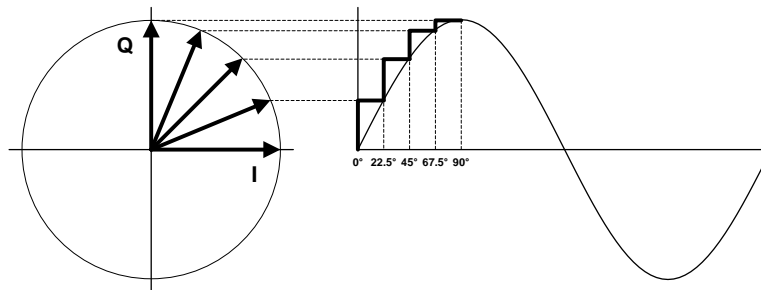


Figure 6.8: Phasors corresponding to a uniform phase step.

In Figure 6.8, the length of the Q vector is modulated according to the sine function. Likewise, the length of the I vector is modulated according to the cosine function (not illustrated). So, the horizontal & vertical components of the phasors are modulated by sinusoidal steps. In other words:

*A uniform phase step requires non-uniform weights for the I & Q vectors.*

This property of a vector modulator was already presented in [Soer et al., 2011], where the weights, modulating the lengths of the I/Q vectors, approximate the sine/cosine curves via a switched-capacitor charge distribution network. In this work the idea, as introduced in section 1.4, is to implement the weights via resistors. According to the circuit specifications, the vector modulator should have a 5-bit uniform phase setting (for comparison purposes).

### 6.5.2 Synthesis of the Weights

To obtain the result of (6.5), the I & Q vectors have to be weighted according to the cosine & sine functions respectively. As shown in Figure 6.1, the vector modulator senses (differential) in-phase & quadrature components of the output voltage of the first TIA stage, i.e.  $V_I$  &  $V_Q$ . Since currents need to be summed at the virtual ground of the second TIA stage,  $V_I$  &  $V_Q$  need to be weighted by resistors, which perform  $V \rightarrow I$  conversion, writing:

$$I = \frac{V_I}{R_I} + \frac{V_Q}{R_Q} \quad (6.6)$$

In order to describe  $R_I$  &  $R_Q$ , a resistor  $R_0$  is defined:

$$R_I = \frac{R_0}{\cos(\varphi)} \quad (6.7a)$$

$$R_Q = \frac{R_0}{\sin(\varphi)} \quad (6.7b)$$

Such that (6.6) becomes:

$$I = \frac{V_I}{R_0} \cos(\varphi) + \frac{V_Q}{R_0} \sin(\varphi) \quad (6.8)$$

Since  $V \rightarrow I$  conversion is performed, i.e. conductance, the inverse of  $R_0$  can be considered the length of the phasor:

$$\frac{1}{R_0} = \sqrt{\left(\frac{1}{R_I}\right)^2 + \left(\frac{1}{R_Q}\right)^2} \quad (6.9)$$

Using (6.7) and a value of  $1207\Omega^1$  for  $R_0$ , gives the values for  $R_I$  &  $R_Q$ , which are listed in Table 6.1:

$R_0 = 1207\Omega$	$R_I[\Omega]$	$R_Q[\Omega]$
$5.625^\circ$	1213	12315
$16.875^\circ$	1261	4158
$28.125^\circ$	1369	2561
$39.375^\circ$	1562	1903
$50.625^\circ$	1903	1562
$61.875^\circ$	2561	1369
$73.125^\circ$	4158	1261
$84.375^\circ$	12315	1213

Table 6.1: Resistor values for  $R_I$  &  $R_Q$  weighting the I/Q signals.

### 6.5.3 Implementation of the Weights

In order to implement the I & Q resistors, their values as presented by Table 6.1 have to be round off. It is assumed that the maximum difference between the smallest and the largest resistance is 6 bit (i.e.  $64\times$ ). A numerical analysis (using Matlab) is performed in order to find a resistor value  $R$ , of which integer multiples approximate the resistor values listed in Table 6.1 with minimal deviation. The analysis results that multiples of  $R = 116\Omega$  yields, on average, the smallest deviation.

Table 6.2 presents the (rounded) values for  $R_I^2$ , using a resistance of  $116\Omega$ .

$R = 116\Omega$	$n$	$nR[\Omega]$	$R_I[\Omega]$	Abs. Error $[\Omega]$	Rel. Error $[\%]$
$5.625^\circ$	10	1160	1213	53	4.37
$16.875^\circ$	11	1276	1261	15	1.19
$28.125^\circ$	12	1392	1369	23	1.68
$39.375^\circ$	13	1508	1562	54	3.46
$50.625^\circ$	16	1856	1903	47	2.47
$61.875^\circ$	22	2552	2561	9	0.35
$73.125^\circ$	36	4176	4158	18	0.43
$84.375^\circ$	100	11600	12315	715	5.81

Table 6.2: Rounded resistor values of  $R_I$ .

<sup>1</sup>The value of  $1207\Omega$  would appear strange. When following a slightly different design procedure, as presented in this section, this value was numerically convenient.

<sup>2</sup> $R_Q$  is not included in Table 6.2, because  $R_I$  &  $R_Q$  are complementary.

### 6.5.4 Proposed Vector Modulator Implementation

The first TIA stage in Figure 6.1, provides voltage outputs. Using resistors to perform  $V \rightarrow I$  conversion, the quadrature vectors (i.e. I/Q currents) are weighted and subsequently summed to obtain the desired phase shift.

Figure 6.9 presents the circuit implementation of the vector modulator.

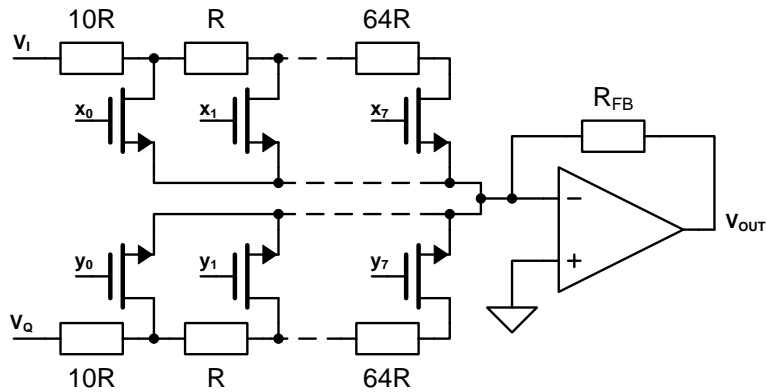


Figure 6.9: Circuit implementation of the vector modulator.

The entire resistor ladder is illustrated in Figure 6.10, synthesizing the values for  $R_I$ . Note that the total resistance accumulates to  $100 \cdot 116 = 11600 \Omega$ .

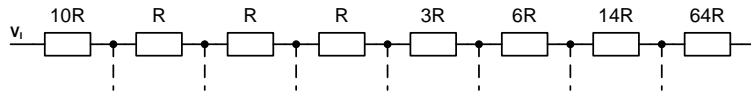


Figure 6.10: Resistor ladder.



# Chapter 7

## Simulation Results

The circuits, as proposed in Chapter 6, are simulated using SpectreRF. These circuits are not optimized to meet a specific design parameter, such as noise, power consumption, etc. The circuits are simulated in order to verify the functional operation of the proposed implementation. This chapter first describes the simulation setup. Subsequent sections present simulation results of the effects of non-linearity; the performance of the vector modulator and finally the interferer rejection.

### 7.1 Simulation Setup

In Figure 6.1, the transconductance of each of the 16 small LNTAs is set to 5 mS. Since 4 of these LNTA currents are summed (to form a Butler beam), an equivalent transconductance of 20 mS is observed, i.e.  $1 \times$  current gain in a  $50 \Omega$  system.

A quad-phase 25 % duty-cycle non-overlapping clock signal is used as local oscillator (LO). The LO signal is used for down conversion. In addition, the LO provides the phases for the Butler BFN. The specifications of the LO are listed in Table 7.1.

Period	1.25 ns
Frequency	800 MHz
Duty-cycle	25 %
Rise-time	50 ps
Fall-time	50 ps
Series resistance	$10 \Omega$

Table 7.1: Specifications of the LO.

Switches are used for the:

- Butler BFN, i.e. the passive mixer blocks.
- Gain (i.e. transimpedance) setting in the first TIA stage.
- Phase setting in the vector modulator.

The switches are implemented using NMOS transistors, with bulk tied to source to avoid body effect. Table 7.2 presents the device properties:

Width	60 $\mu\text{m}$
Length	0.06 $\mu\text{m}$
Fold	60
On resistance	8 $\Omega$
Bulk-Source voltage	0 V

Table 7.2: Device properties of an NMOST.

## 7.2 Gain Compression

Since voltage gain is avoided at RF, the *gain compression* of the first TIA stage is an important measure to indicate what power level can be processed. Therefore, the 1 dB compression point (CP) is a suitable figure to characterize the linearity of the front-end.

Consider the case that a strong interferer is fully captured in one Butler beam. In that case, all interference current is processed over one path of the receiver. In order to *null* this interferer, the gain setting (i.e. the transimpedance) of the involved TIA stage is set to the lowest value ( $a_0$ ). As shown in Figure 6.4, this implies that the interference current is simply dumped to ground.

However, it could occur that the interferer is not fully captured by a Butler beam, but for about 95%. In that case, the beamforming algorithm will result a magnitude weight unequal to zero, for the involved TIA stage. So, not the lowest gain setting ( $a_0$ ), but one setting higher (i.e.  $a_1$ ) is used. In this case, still a considerable amount of (interference) current has to be processed by the involved TIA stage.

An interferer located at  $u = 0.04$ , is such a case. The algorithm results gain setting  $a_1$  for the center beam. This can be considered a worst-case scenario in terms of gain compression. Figure 7.1a presents the compression curve for this scenario, resulting a 1 dB, input-referred CP of -8.34 dBm. The 1 dB

output-referred CP is -8.65 dBm. When the Op-Amp cannot sink/source the input current, due to a low feedback resistance, internal clipping can occur. This is probably the case when setting  $a_0$ .

Figure 7.1b presents the compression curve in case of no interference, such that all signals can be processed with maximum gain. The simulation yields a 1 dB, input-referred CP of -8.81 dBm and a 1 dB output-referred CP of 6.69 dBm.

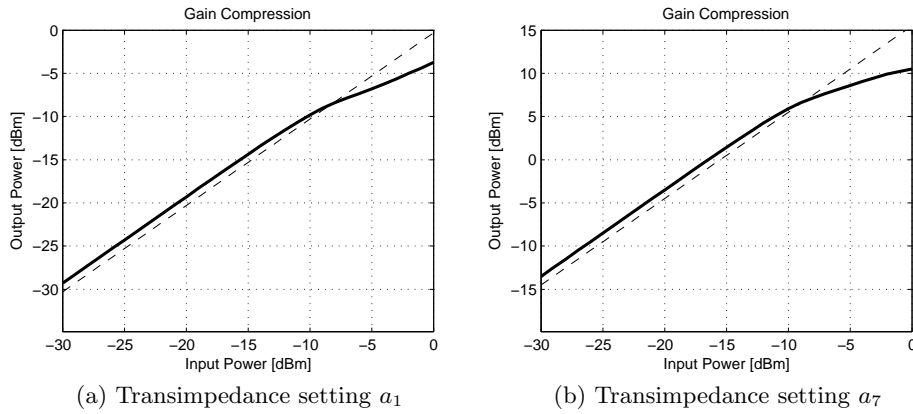


Figure 7.1: Compression curves for 2 transimpedance settings.

### 7.3 Third-Order Intermodulation Distortion

Intermodulation (IM) products limit the linearity of the implemented beamforming system. The linearity of the proposed circuits is examined by simulating the third-order intercept point (IP3). A circuit simulation of the implemented broadside Butler BFN, demonstrates an input-referred third-order intercept point (IIP3) of 26.83 dBm. This high IIP3 is due to high linearity offered by passive mixers [Ru et al., 2009]. The first TIA stage is linearized by negative feedback and demonstrates an IIP3 of 11.98 dBm. The Butler BFN together with the first TIA stage show an IIP3 of -1.06 dBm.

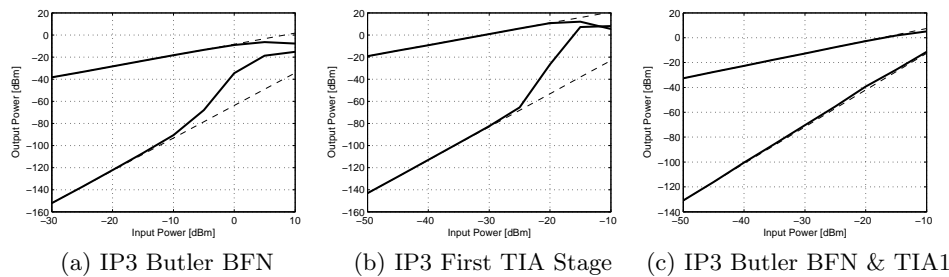


Figure 7.2: IP3 plots.

## 7.4 Vector Modulator

Figure 7.3 presents the phase shifts provided by the vector modulator. For higher frequencies, the curves start to bend. This can be viewed as a rotation of the constellation points in a phasor diagram. Though, the relative phase difference, between two successive phase settings, remains constant. This is more clearly seen, when the phases are plotted on a linear frequency scale.

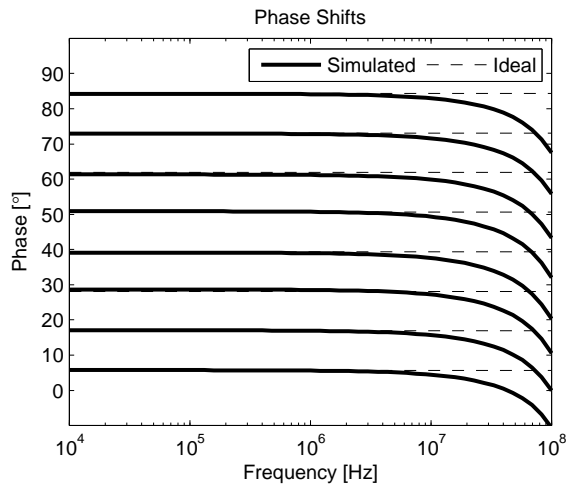


Figure 7.3: Phase shifts provided by the vector modulator.

Figure 7.4 presents the phase and magnitude errors of the vector modulator. These errors are the result of quantization. Simulations result an RMS phase error of  $0.32^\circ$  and an RMS magnitude error of 0.22 dB.

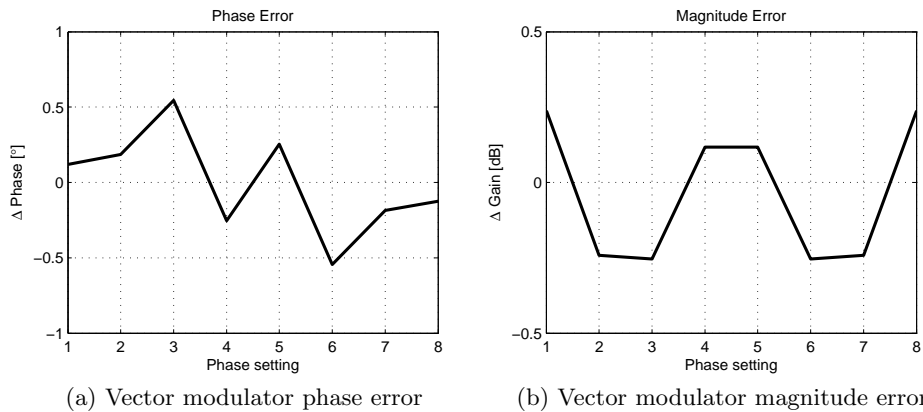


Figure 7.4: Phase & magnitude errors due to quantization.

## 7.5 Nulling Performance

In order to verify the nulling performance of the implemented beamforming system, two scenarios are examined, i.e.:

- Worst-case interference rejection after the 1<sup>st</sup> TIA stage.
- Worst-case interference rejection after the 2<sup>nd</sup> TIA stage (i.e. the vector modulator).

The beamforming algorithm provides the interferer position and the corresponding rejection for each cases, which are summarized in table 7.3.

TIA stage	Interferer position	Rejection [dB]
1 <sup>st</sup>	$u = -0.86$	9.22
2 <sup>nd</sup>	$u = -0.37$	22.02

Table 7.3: Worst-case rejections determined by the algorithm.

Figure 7.5 presents the weighted Butler beams, in case an interferer is located at  $u = -0.86$ . The Butler beam, which is maximal at this position, serves as a measure for the SIR improvement. From Figure 7.5, it follows that beam 1R (in blue), which is shifted to  $u = -1$  to approach the interferer, has the largest magnitude at  $u = -0.86$ . The SpectreRF simulation results a SIR improvement of 7.36 dB.

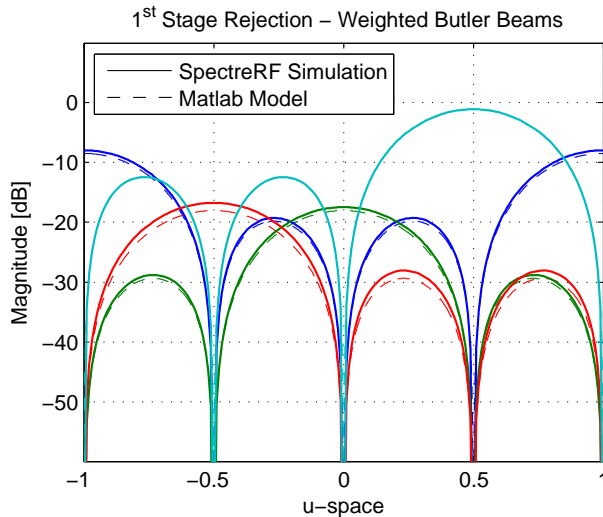


Figure 7.5: 1<sup>st</sup> stage worst-case rejection,  $u_{int} = -0.86$ .

Note that the main beam (in cyan) in Figure 7.5, does not peak to 0 dB. This is due to the maximal quantization value, which is set to 0.875. Consequently, the main beam peaks to:

$$0 \text{ dB} - 20 \log \left( \frac{1}{0.875} \right) = -1.16 \text{ dB}$$

Figure 7.6 presents the interference nulled radiation pattern, i.e. the rejection after the vector modulator. At  $u = -0.37$ , a rejection of 17.56 dB is observed.

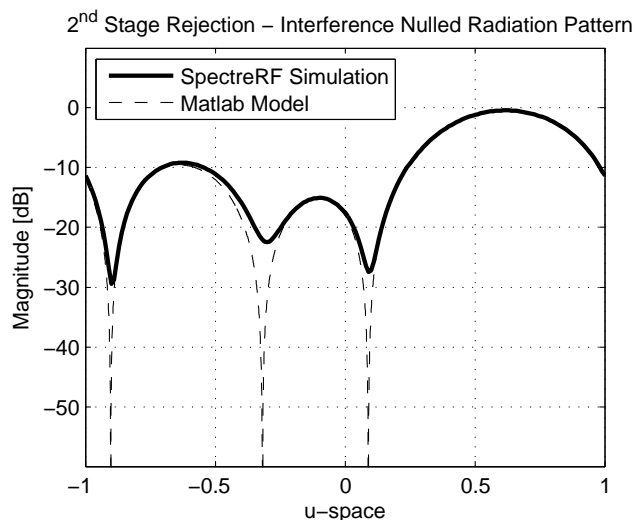


Figure 7.6: 2<sup>nd</sup> stage worst-case rejection,  $u_{int} = -0.37$ .

## 7.6 A Word about Noise

As mentioned before, the proposed circuits are not optimized for noise. If only the Butler BFN, the first TIA stage and the vector modulator are considered, the largest contributor of noise is the vector modulator. This is because the weighting network of the vector modulator consists of resistors, which add a noise voltage to the input voltage. Since noise power ( $\overline{V_n^2} = 4kTR$ ) linearly increases with resistance, high impedance levels yield major noise contributions.

## 7.7 Power Consumption

The implemented beamforming system draws 39.61 mW from a 1.2 V supply.

## Chapter 8

# Conclusions

- The beams of a *Butler Matrix* beamforming network (BFN) can be used to 'capture' and reject an interferer. A beamforming algorithm, utilizing these Butler beams, can be used to solve the *complex weights*, which yield a SIR & SNR improved radiation pattern.
- Evaluations of the system model show, that forcing a *null* at different angular positions, results a small loss of gain for the main beam.
- A passive down-conversion mixer, driven by a non-overlapping 25% duty-cycle clock signal, can be used to implement a *Broadside Butler* BFN. When the passive mixer operates in the current domain, the phase-shifted & down-converted signals can be summed at the virtual ground of a transimpedance amplifier (TIA) stage, to form a Butler beam.
- A circuit implementation based on Op-Amps & resistors is suitable for synthesizing the complex weights of a linear array antenna. The magnitudes and phases of these complex weights can be separately implemented over two TIA stages, such that an orthogonal mapping of complex weights to a circuit implementation is possible.
- A TIA stage can be used to implement the magnitude weights, weighting the Butler beams in order to provide a first-stage interference rejection.
- A *vector modulator* can be constructed using NMOS switches, resistors and an Op-Amp in order to implement a phase shifter. Circuit simulations demonstrate an RMS phase error of  $0.32^\circ$  and an RMS magnitude error of 0.22 dB, due to the quantization of the used resistor.

- Circuit simulations demonstrate a first-stage interferer rejection of 7.36 dB (worst-case). A second stage demonstrates a worst-case rejection of 17.56 dB. System model and circuit simulations show good correspondence.
- The number of phases, used for the Butler BFN, and the number of quantization bits dictate the nulling performance. For low resolutions (i.e. large quantization steps), process spread and device mismatch are of less concern, since the used quantization steps are larger than these variations.

## Chapter 9

# Recommendations

- Consider the case that the TIA goes into compression and the output voltage does not clip to the supply. It could be investigated if a larger current drive of the Op-Amp can avoid compression. In addition, it can be investigated if the linearity of the used Op-Amp can be improved, or that another design yields better results in terms of linearity/compression.
- The way in which quantization is applied to the magnitude weights, can be investigated. In this work, a uniform distribution of quantization levels is used, for linear gain setting. However, the beamforming algorithm rarely results magnitude weights  $a_3, a_4$  &  $a_5$ , i.e. the center values. It could be that these values can be omitted, such that more quantization levels can be used for the higher & lower gain settings, using the same number of bits.
- Consider the case that the first TIA stage provides a minimum rejection of 30 dB (using more phases for the Butler BFN & more bits for the magnitude weights), such that a 0 dBm interferer is attenuated to the signal level. In that case, an analog-to-digital converter (ADC) can be placed directly after the TIA stage, such that phase shifting & beam summation can be performed in the digital domain.



# Bibliography

- R. Jacob Baker. *CMOS Circuit Design, Layout, and Simulation*. IEEE Press Series on Microelectronic Systems. John Wiley & Sons, Inc., third edition, 2010. ISBN 978-0-470-88132-3.
- Jesse L. Butler and Ralph Lowe. Beam-Forming Matrix Simplifies Design of Electronically Scanned Antennas. *Electronic Design*, 9:170–173, April 12 1961.
- Robert C. Hansen. *Phased Array Antennas*. Wiley Series in Microwave and Optical Engineering. John Wiley & Sons, Inc., second edition, 2009. ISBN 978-0-470-40102-6.
- John Litva and Titus Kwok-Yeung Lo. *Digital Beamforming in Wireless Communications*. The Artech House Mobile Communications Series. Artech House, Inc., August 1996. ISBN 978-0-89006-712-3.
- Robert J. Mailloux. *Phased Array Antenna Handbook*. Artech House Antennas and Propagation Library. Artech House, Inc., second edition, 2005. ISBN 978-1-58053-689-9.
- Louie Pylarinos. Charge Pumps: An Overview. University of Toronto. URL <http://citeseerx.ist.psu.edu/viewdoc/summary?doi=10.1.1.128.4085>.
- Kuba Raczkowski, Walter De Raedt, Bart Nauwelaers, and Piet Wambacq. A Wideband Beamformer for a Phased-Array 60GHz Receiver in 40nm Digital CMOS. In *IEEE International Solid-State Circuits Conference - Digest of Technical Papers, ISSCC 2010*, pages 40–41, February 2010. URL <https://lirias.kuleuven.be/handle/123456789/286167>.
- Harish Rajagopalan. Design and Implementation of Butler Matrix - Simultaneous Beam Formation, August 2006. URL <http://www.ee.ucla.edu/~harish/index.html>.
- Behzad Razavi. *Design of Analog CMOS Integrated Circuits*. McGraw-Hill Series in Electrical and Computer Engineering. McGraw-Hill, international edition, 2001. ISBN 978-0-07-118839-5.

## BIBLIOGRAPHY

---

- Zhiyu Ru, Niels A. Moseley, Eric A.M. Klumperink, and Bram Nauta. Digitally Enhanced Software-Defined Radio Receiver Robust to Out-of-Band Interference. *IEEE Journal of Solid-State Circuits*, 44(12):3359–3375, December 2009. URL <http://doc.utwente.nl/69829/>. Special Issue on the 2009 IEEE International Solid-State Circuits Conference, ISSCC in San Francisco, CA, February 2009.
- Michiel C.M. Soer, Eric A.M. Klumperink, Bram Nauta, and Frank E. van Fliet. A 1.0-to-4.0GHz 65nm CMOS Four-Element Beamforming Receiver using a Switched Capacitor Vector Modulator with Approximate-Sine Weighting. In *IEEE International Solid-State Circuits Conference - Digest of Technical Papers, ISSCC 2011*, February 2011.
- Hubregt J. Visser. *Array and Phased Array Antenna Basics*. John Wiley & Sons, Ltd, 2005. ISBN 978-0-470-87117-1.
- Hua Wang and Ali Hajimiri. A Wideband CMOS Linear Digital Phase Rotator. In *IEEE Custom Integrated Circuits Conference (CICC)*, pages 671–674, September 2007. URL [http://www.its.caltech.edu/~hajimiri/pdf/Wang\\_CICC\\_2007.pdf](http://www.its.caltech.edu/~hajimiri/pdf/Wang_CICC_2007.pdf).